The role of fluid pressure and diagenetic cements for porosity preservation in Triassic fluvial reservoirs of the Central Graben, North Sea

Binh T. T. Nguyen, Stuart J. Jones, Neil R. Goulty, Alexander J. Middleton, Neil Grant, Alison Ferguson, and Leon Bowen

ABSTRACT

Anomalously high porosities and permeabilities are commonly found in the fluvial channel sandstone facies of the Triassic Skagerrak Formation in the central North Sea at burial depths greater than 3200 m (10,499 ft), from which hydrocarbons are currently being produced. The aim of our study was to improve understanding of sandstone diagenesis in the Skagerrak Formation to help predict whether the facies with high porosity may be found at even greater depths. The Skagerrak sandstones comprise fine to medium-grained arkosic to lithic-arkosic arenites. We have used scanning electron microscopy, petrographic analysis, pressure history modeling, and core analysis to assess the timing of growth and origin of mineral cements, with generation, and the impact of high fluid pressure on reservoir quality. Our interpretation is that the anomalously high porosities in the Skagerrak sandstones were maintained by a history of overpressure generation and maintenance from the Late Triassic onward, in combination with early microquartz cementation and subsequent precipitation of robust chlorite grain coats. Increasing salinity of pore fluids during burial diagenesis led to pore-filling halite cements in sustained phreatic conditions. The halite pore-filling cements removed most of the remaining porosity and limited the precipitation of other diagenetic phases. Fluid flow associated with the migration of hydrocarbons during the Neogene is inferred

Manuscript received November 2, 2011; provisional acceptance February 2, 2012; revised manuscript received August 31, 2012; final acceptance January 15, 2013.
DOI:10.1306/01151311163

AUTHORS

BINH T. T. NGUYEN ~ *Department of Earth Sciences, Durham University, Durham, United Kingdom; thi.thanh.binh.nguyen@nex.jx-group.co.jp*

Binh Nguyen received her B.Sc. degree in geophysics from Hanoi University and her M.Sc. degree and Ph.D. from the University of Tokyo. She was a postdoctoral researcher at Durham University from 2008 to 2011, where she specialized in pore-pressure and fluid-flow evolution in sedimentary basins. She has recently joined JX Nippon Oil & Gas Exploration Corporation as a senior geologist in Tokyo.

STUART J. JONES ~ *Department of Earth Sciences, Durham University, Durham, United Kingdom; stuart.jones@durham.ac.uk*

Stuart Jones is a lecturer in sedimentology at Durham University. He holds a B.Sc. degree in geology from Aberystwyth University and a Ph.D. in sedimentology from the University of Reading. His research interests lie in the area of siliciclastic depositional systems and their diagenesis and, in particular, applying this to reservoir characterization.

NEIL R. GOULTY ~ *Department of Earth Sciences, Durham University, Durham, United Kingdom; n.r.goulty@durham.ac.uk*

Neil Goulty is a professor at Durham University. His principal research interests are in geomechanical processes in sedimentary basins, with current focus on the compaction of mudrocks and overpressure.

ALEXANDER J. MIDDLETON ~ *ConocoPhillips Norway, Stavanger, Norway; Jamie.Middleton@conocophillips.com*

Alexander J. Middleton is an exploration geologist at ConocoPhillips Norge with more than 30 years of industry experience. He received his B.Sc. degree in geology from the University of London.

NEIL GRANT ~ *ConocoPhillips Petroleum Exploration Company UK, Ltd., Rubislaw House, Anderson Drive, Aberdeen, United Kingdom; Neil.T.Grant@conocophillips.com*

Neil Grant is a structural geologist working for ConocoPhillips UK, Ltd., in Aberdeen, Scotland. He has a B.Sc. degree in applied geology from the University of Strathclyde and a Ph.D. from Leeds

University. He has worked for 23 years in the industry. His principal interests are in exploration geology.

ALISON FERGUSON ~ *ConocoPhillips Norway, Stavanger, Norway; Alison.Ferguson@conocophillips.com*

Alison Ferguson has been a geologist with ConocoPhillips for almost 10 years. She received her B.Sc. (hons) from Queen's University Belfast, and her M.Sc. degree from Royal Holloway, University of London.

LEON BOWEN ~ *Department of Physics, Durham University, Durham, United Kingdom; leon.bowen@durham.ac.uk*

Leon Bowen is an advanced electron microscopist. He received his first degree in forensic engineering and his M.B.A. degree in industrial management from Sheffield Hallam University. His current research focuses on material characterization techniques and failure analysis using electron microscopy.

ACKNOWLEDGEMENTS

This research was funded by ConocoPhillips, BG Group, and Talisman Energy. Beicip are acknowledged for providing a TEMISpack academic license and technical support. We thank AAPG Editor Stephen Laubach for his suggestions and reviewers Linda Bonnell, Gary Couples, and an anonymous reviewer for their meticulous and constructive review of the article.

The AAPG Editor thanks the following reviewers for their work on this paper: Linda M. Bonnell and Gary D. Couples.

to have dissolved the halite locally. Dissolution of halite cements in the channel sands has given rise to megapores and porosities of as much as 35% at current production depths.

INTRODUCTION

Fluvial sandstones commonly display complex internal geometries and architectures, making them particularly difficult reservoirs to develop. Typically, channelized sand bodies have complicated diagenetic histories because of their varied lithology and textural maturity and their close association with fine-grained floodplain and/or lacustrine facies (Hammer et al., 2010; Morad et al., 2010; Willis and Tang, 2010).

The Triassic Skagerrak Formation in the North Sea Central Graben (Figure 1) is a fluvial system deposited in tectonically active half grabens where episodic basin-floor subsidence and growth faulting controlled sedimentation. The Skagerrak Formation is further complicated by Triassic halokinesis of the underlying Permian Zechstein salts creating many salt withdrawal minibasins or pods (Hodgson et al., 1992; Smith et al., 1993; Penge et al., 1999; Davison et al., 2000; Archer et al., 2010). These pods were filled with nonmarine sedimentation of the Smithbank and Skagerrak Formations, reaching thicknesses of as much as 2 km (1 mi) (Goldsmith et al., 1995, 2003). Skagerrak fluvial sedimentation during the Middle to Late Triassic (Ansian to Rhaetian) occurred in coexisting braided and meandering channels together with playa and lacustrine deposition (Hoiland et al., 1993; Goldsmith, et al., 1995, 2003; Fisher and Mudge, 1998; de Jong et al., 2006; Lervik, 2006).

The Triassic Skagerrak Formation is one of the main reservoirs in the high pressure–high temperature (HPHT) province in the Central Graben. Pore pressures can exceed 80 MPa (11,603 psi) in the upper part of the Skagerrak Formation at depths of 4000 to 5000 m (13,123–16,404 ft) below seafloor, where temperatures are in the range of 166°C to 200°C (Swarbrick et al., 2000; Primio and Neumann, 2008). Overpressures are widespread in the Mesozoic reservoirs in the central North Sea, a region that since the early Cretaceous has experienced almost continuous sedimentation of dominantly fine-grained lithologies (Osborne and Swarbrick, 1999; Swarbrick et al., 2000; Yardley and Swarbrick, 2000; Primio and Neumann, 2008).

The Skagerrak fluvial channel sandstones possess remarkably good porosity, as much as 35%, with respect to their present-day depths of burial (Figure 2). Previous studies of mechanisms to maintain anomalously high porosities in reservoir sandstones

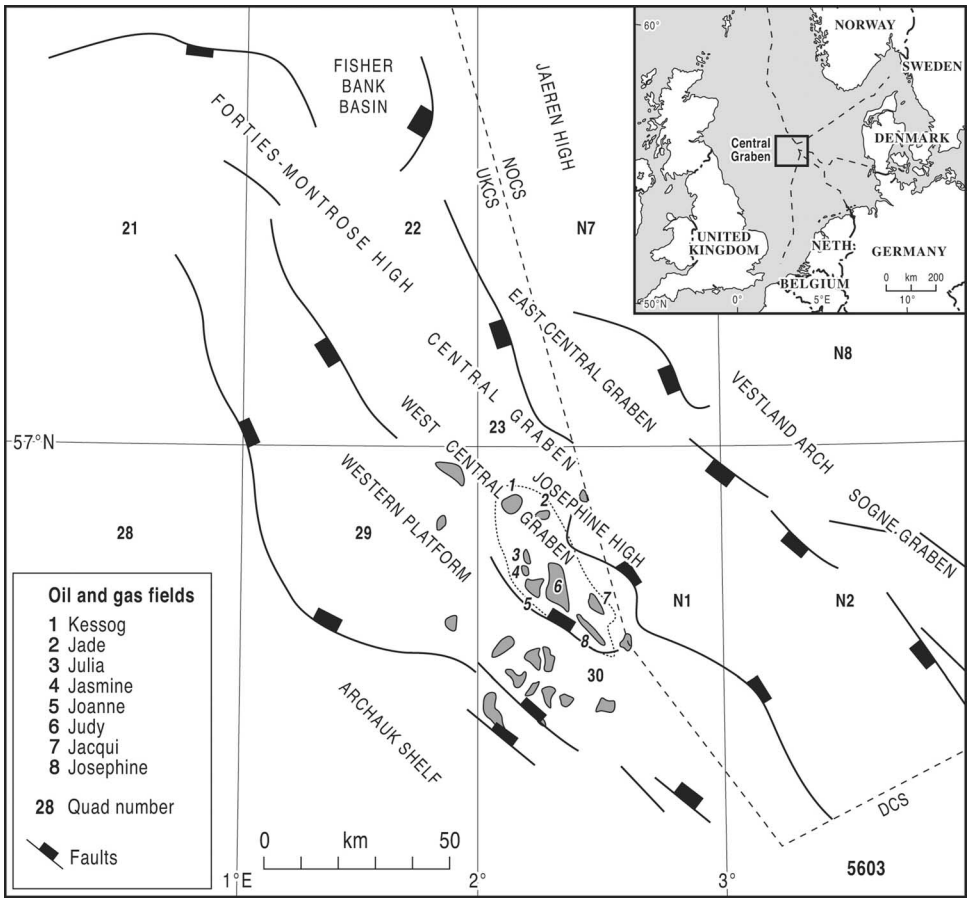

Figure 1. Location map of the central North Sea, United Kingdom, showing quad 30 (J Block) and the oil and gas fields used in this study. The United Kingdom continental shelf (UKCS), Norway continental shelf (NOCS), and Danish continental shelf (DCS) boundaries are shown for reference.

have ascribed the inhibition of cementation to the early emplacement of hydrocarbons, grain coatings, secondary porosity related to dissolution of framework grains and/or cements, and lateral fluid flows (e.g., Smith et al., 1993; Haszeldene et al., 1999; Bloch et al., 2002; Taylor et al., 2010). These studies did not directly use the pressure history and its possible interrelationship with diagenesis as a control on

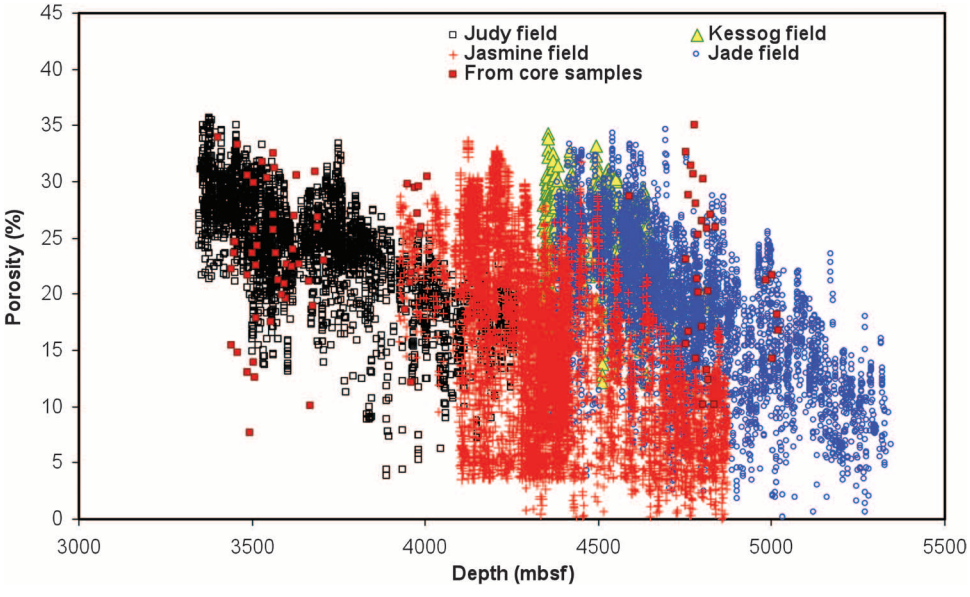

Figure 2. Porosity measurements plotted against depth for core samples (red squares) and density logs (other symbols) from Skagerrak reservoirs in J Block, United Kingdom quad 30.

porosity. This was in part because quantitative pressure modeling is commonly hindered by the lack of pressure constraints in the past and insufficient knowledge of sediment porosity and permeability evolution from the time of deposition.

Here, we present new results for the diagenetic evolution of the Triassic Skagerrak Formation in the Josephone high (J Block), located within the Central Graben in United Kingdom (UK) quad 30 (Figure 1). Generation of pore-fluid pressures in the Late Triassic contributed to the maintenance of high primary porosities and influenced the diagenesis of the Skagerrak Formation. It has been possible to compare the calculated paleopressures with detailed petrographic analyses of the reservoir sandstones that preserve high primary porosities from the Late Triassic to the present day. The approach presented in this article provides an important step toward predicting whether high porosities may be found in Triassic reservoir sandstones at greater depths in the Central Graben.

GEOLOGIC SETTING OF THE CENTRAL GRABEN

The Central Graben forms the southern arm of a trilete rift system (i.e., an incipient ridge-ridge triple junction) in the North Sea, with the Viking Graben as the northern arm and the Moray Firth Basin as the western arm. It is a 70 to 130 km (43–81 mi) wide graben with a length of approximately 550 km (342 mi). At least two major rifting phases, one during the Permian-Triassic (290–210 Ma) and the second during the Late Jurassic (155–140 Ma), were important factors in the development of the Central Graben rift system (Gowers and Sæbøe, 1985; Hoiland et al., 1993; Glennie, 1998). The geologic history is commonly divided into prerifting, synrifting, and postrifting phases (Clark et al., 1999). Synrift sediments are siliciclastic Triassic and Jurassic sediments of as much as 2000 m (6562 ft) in thickness. The postrift sediments from the Cretaceous to the Holocene are as much as 4500 m (14,764 ft) in thickness. Postrift sediments are mainly siliciclastic rocks dominated by shale, sandstones, silty sandstone, and a thick chalk section (Goldsmith et al., 2003).

Our study focuses on the HPHT sections in the Josephine High (Figure 1). This area forms part of a wider HPHT province that includes the Triassic strata of the Central Graben and the southern part of the Viking Graben (Goldsmith et al., 2003; Lervik, 2006). The stratigraphy, structural development, and overpressure development are summarized here to provide a regional context for the descriptions and interpretations of the Skagerrak Formation diagenesis that follow.

Skagerrak Stratigraphy and Pod Development

The Triassic Skagerrak Formation consists of some 500 to 1000 m (1640–3281 ft) of predominantly continental braided and meandering fluvial systems and terminal fluvial fans with lacustrine facies (McKie and Audretsch, 2005; de Jong et al., 2006). The stratigraphic nomenclature for the Triassic of the Central Graben was proposed by Goldsmith et al. (1995) and is based on biostratigraphic and lithostratigraphic methods, including wireline-log correlations. The formation contains three major sand-prone successions—the Judy, Joanne, and Josephine Sandstone Members—intercalated with siltstone-mudstone successions of the Julius, Jonathan, and Joshua Mudstone Members (Figure 3). The fluvial sandstone reservoir facies includes sheetflood and crevasse splay deposits in addition to multistorey stacked channel sandbodies (Goldsmith et al., 1995, 2003; McKie and Audretsch, 2005). The mudstones constitute nonreservoir floodplain, lacustrine, and playa facies.

The exact relationship between the reservoir and nonreservoir facies (fluvial-lacustrine interaction) is not clear, but the Central Graben was probably an internally draining basin during the Triassic where, in the absence of eustatic controls, climate and tectonics were the key drivers for sedimentation. The climate during the Triassic fluctuated through varying levels of aridity and humidity, with the dispersal of sand into these basins dependant on catchment runoff from the basin flanking regions. (Smith et al., 1993; Cartwright et al., 2001; McKie and Williams, 2009). This fluctuating climate has been recognized as a significant factor in controlling the sandstone and mudstone cyclicity

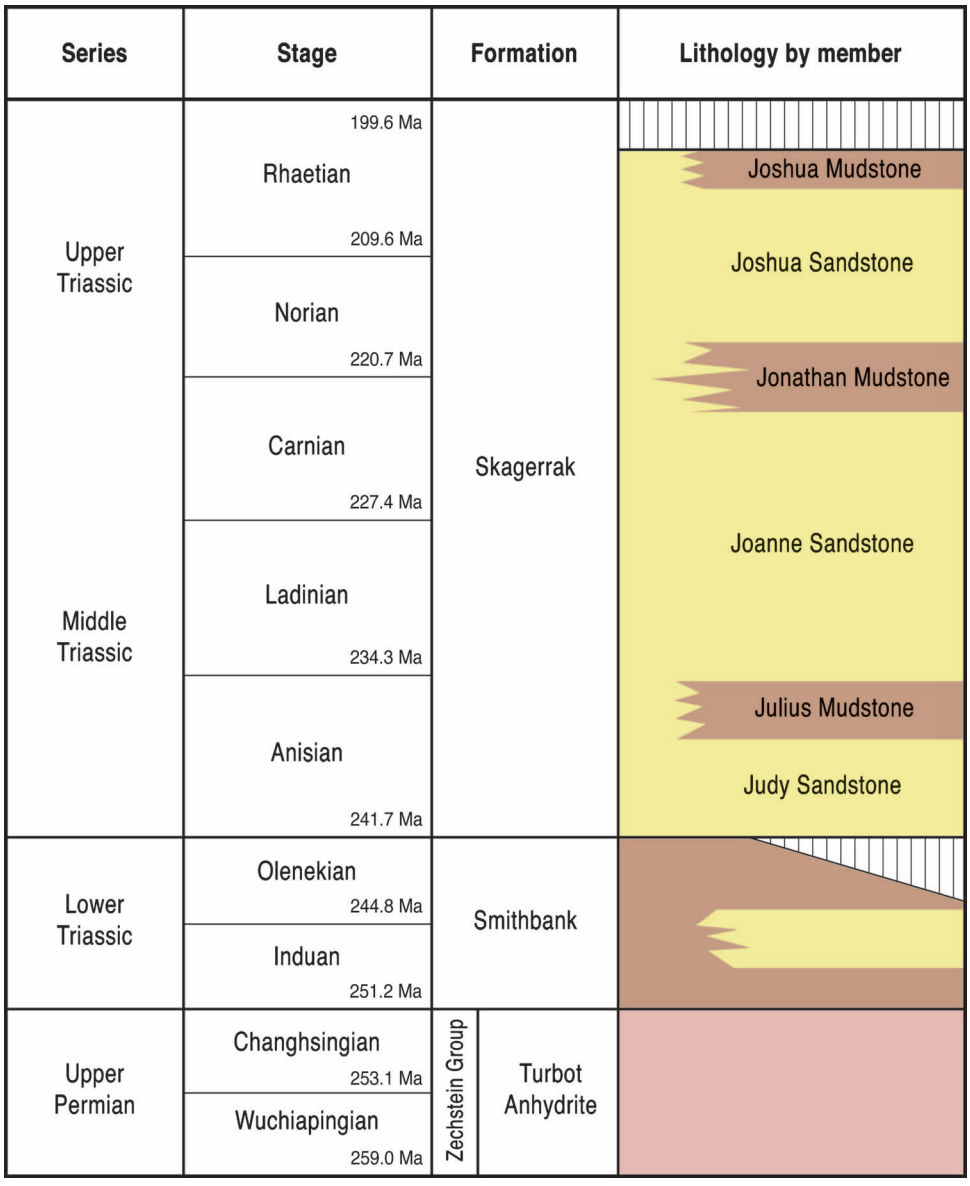

Figure 3. General stratigraphy of the study area (modified from Goldsmith et al., 2003; McKie and Williams, 2009).

(Goldsmith et al., 2003; N. Meadows, 2011, personal communication).

The Skagerrak Formation accumulated in a series of fault- and salt-controlled minibasins, or pods, within the overall rift basin (Hodgson et al., 1992; Smith et al., 1993; Matthews et al., 2007). The thick Permian Zechstein salt underlying the Central Graben strongly influenced sedimentation by forming salt withdrawal basins caused by a combination of structural extension and loading (Smith et al., 1993; Bishop, 1996; Matthews et al., 2007; Jackson, et al., 2010). Pod development was active throughout the Triassic, and the Skagerrak is found in the upper part of pods and is commonly preserved between pods. In the study area, the pods provided localized depocenters for the southeasterly flowing Skagerrak fluvial system and were mostly responsible for increasing the preservation potential of the sediments relative to interpod areas.

Present-Day Pressure Distribution

The pore pressure–depth profile in the Central Graben contains an overpressure transition zone of 5 to 10 MPa (725–1450 psi) in the Upper Cretaceous Chalk (Gaarenstroom et al., 1993; Darby et al., 1996;

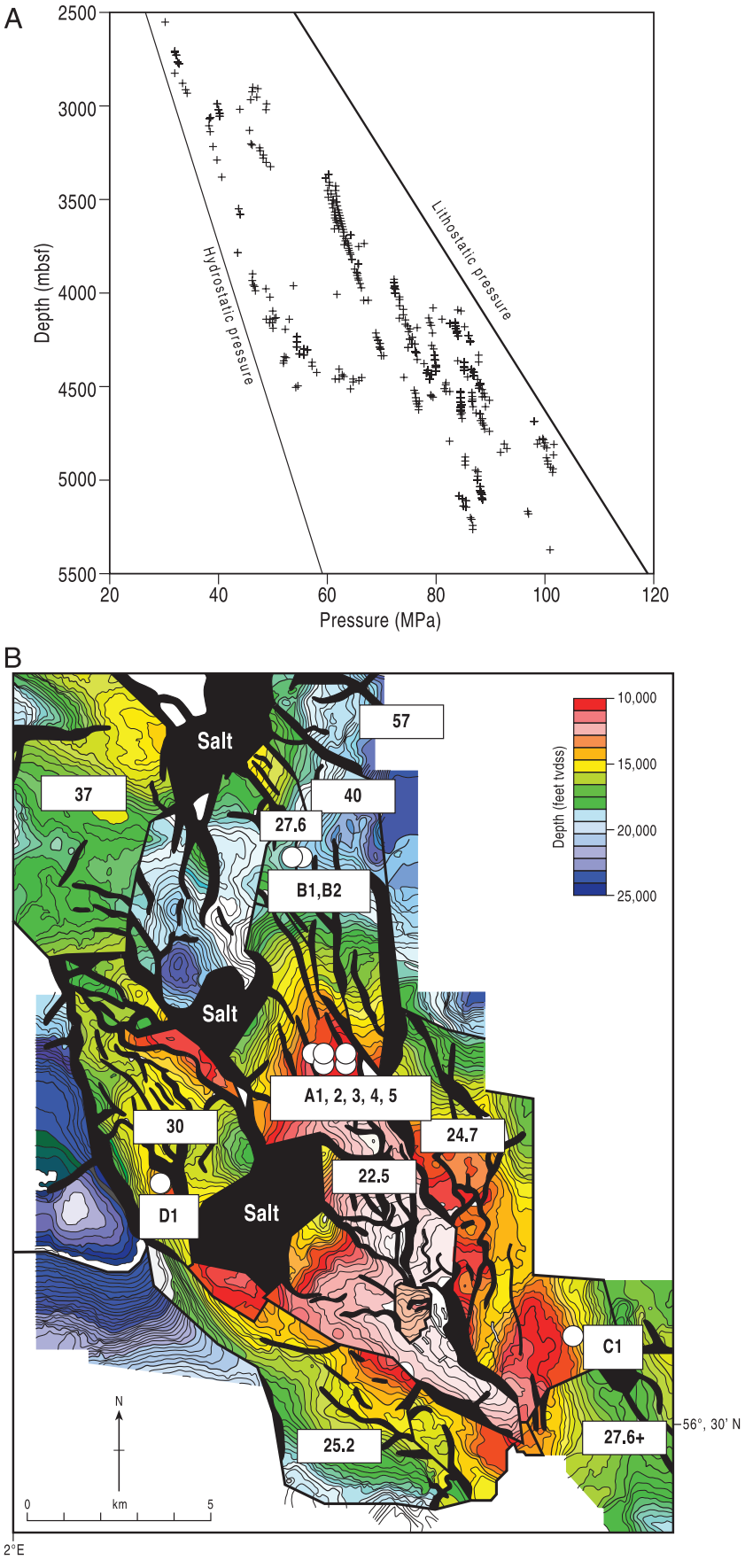

Figure 4. (A) Composite plot of pore pressure against depth for Triassic formations in United Kingdom quad 30. Data are obtained from 3000 modular formation dynamics tester (MDT) and drill stem test (DST) tests in 41 wells. Hydrostatic pressure was calculated assuming that the formation water density is 1.1 g cm^{-3}. (B) Top Triassic depth map for J Block with known pressure cell boundaries marked in white and aquifer overpressures labeled (in megapascal). The core samples used in this study came from wells labeled A1 (30/7a-7), A2 (30/7a-8), A3 (30/7a-9), A4 (30/7a-11z), A5 (30/7a-P3), B1 (30/2C-4), B2 (30/2C-J7), C1 (30/13-5), and D1 (30/6-7).

Table 1. List of Wells Where We Have Run One-Dimensional Basin Modeling, with Numbers of Bulk Rock Samples and Thin Sections Used for Scanning Electron Microscope/Energy-Dispersive Detector, Modal, and Image Analysis

Well	Number of Bulk Rocks	Number of Thin Sections	Depth Interval (mbsf)	Effective Stress (MPa)	Member
30/7a-7	37	16	3104.5–3516.5	11.9–13.3	Jonathan, Judy, Julius
30/7a-8	7	17	3401.6–3638.3	12.8–16.0	Joanne
30/7a-9		7	3630.5–3708.5	13.0–15.0	Joanne
30/7a-11Z	6	6	3486.6–3561.1	10.7–16.0	Joanne
30/7a-P3	1	7	3948.5–4006.7	14.2–15.5	Judy
30/2C-4	29	18	4589.4–4813.5	21.4–22.7	Joanne
30/2C-J7	11	5	4983.6–5019.4	19.3–20.0	Joanne
30/13-5	20	17	3943.9–3996.4	14.0–16.6	Joanne
30/6-7	6	7	4789.6–4837.0	11.4–11.6	Joanne, Julius
9 wells	**117**	**100**	**3104.5–5019.4**	**10.7–22.7**	

Holm, 1998; Osborne and Swarbrick, 1999). The highly overpressured sub-Cretaceous reservoirs at burial depths of 4000 to 5000 m (13,123–16,404 ft) are of Triassic and Middle Jurassic age (Skagerrak Formation and Brent Group, respectively), and temperatures range from 150°C to 195°C. Reservoir pore pressures can exceed 80 MPa (11,603 psi), that is, in the Triassic reservoirs of the Jade and Judy fields (Swarbrick et al., 2000; Primio and Neumann, 2008). Triassic overpressures have previously been thought to be the same as in the overlying Jurassic pressure compartments (Haszeldene et al., 1999). However, more recent studies (e.g., Lines and Auld, 2004; Kape et al., 2010) of pore pressure have identified the variability between different sandstone members in the Skagerrak Formation and, unlike the Jurassic, no areas exist where the Triassic pore pressures are hydrostatic (Figure 4A).

Overpressure magnitudes in Triassic Skagerrak reservoirs differ between pods (Figure 4B). Even intrapod, the overpressure distribution in water-saturated reservoirs can change across faults and across mudstone beds. The magnitude of overpressure in the J Block study area shows a general trend of decreasing overpressure from the deeper Central Graben axis (e.g., 35 MPa [5076 psi] in the Jade field and 40 MPa [5802 psi] in the Kessog field at 4900 mbsf) to the margins in shallower flanking structures and structural highs (e.g., 25–27 MPa [3626–3916 psi] in the Judy field at 4300 mbsf) (Jones et al., 2004; Lines and Auld, 2004).

The main mechanisms recognized for overpressure generation in the Skagerrak Formation have been thought to be disequilibrium compaction, caused by rapid burial during the late Neogene, and hydrocarbon generation, particularly late-stage gas cracking in deep source kitchens for the last 5 to 10 m.y. (Osborne and Swarbrick, 1999; Swarbrick et al., 2000; Isaksen, 2004; Primio and Neumann, 2008). However, we have inferred from one-dimensional modeling, as described below, that important phases of overpressure generation by disequilibrium compaction occurred early in the burial history of the Triassic Skagerrak Formation and have been an important factor in controlling the diagenetic evolution of the reservoirs.

OVERPRESSURE HISTORY FROM ONE-DIMENSIONAL MODELING

Previous studies of overpressure generating mechanisms have concentrated on the high-magnitude phases of development during the Neogene and the latest burial events. They have identified the need for a combination of mechanisms (gas generation and disequilibrium compaction) to generate overpressures of as much as 40 MPa (5802 psi) in the Central Graben HPHT province (e.g., Primio and Neumann,

Table 2. Input Parameters for One-Dimensional Basin Modeling*

(A)

Facies	Initial Porosity (%)	c (MPa^{-1})
Confining channel sandstone	45.0	0.039
Sheetflood sandstone	40.0	0.032
Shale	55.0	0.055
Chalk	42.5	0.036
Salt	0.5	0.001

(B)

Lithology Type	A	B
Clays and shale	0.15	–9.5
Silty clays	0.15	–6
Eocene/Paleocene sandstones	0.14	–2.2
Reservoir chalk	0.06	–1.97
Nonreservoir chalk	0.04	–9.1
Triassic and Jurassic sandstones	0.15	–2.2
Salts	0.15	–13

(C)

				Thickness (m) and Lithology (%)**			
Layer	Start Time (Ma)	End Time (Ma)	Formation	30/2C-4		30/7a-7	
Layer 1	3.5	0	Nordland 1	400	Clays	350	Clays
Layer 2	5.2	3.5	Nordland 2	400	Clays	300	Clays
Layer 3	24	5.2	Nordland 3	1000	Clays	1000	Clays
Layer 4	33.5	24	Nordland 4	550	Shales	528.4	Shales
Layer 5	53	33.5	Hordaland 1	570	Shales	550	Shales
Layer 6	55	53	Hordaland 2	114	30% sst; 70% shale	100	30% sst; 70% shale
Layer 7	57.9	55	Balder	21.7	50% sst; 50% shale	16.1	50% sst; 50% shale
Layer 8	58.5	57.9	Sele	38.3	50% sst; 50% shale	54.8	50% sst; 50% shale
Layer 9	60	58.5	Andrew-Lista	96.5	50% sst; 50% shale	43.4	50% sst; 50% shale
Layer 10	61	60	Maureen	133.7	50% sst; 50% shale	110.1	50% sst; 50% shale
Layer 11	65	61	Ekofisk	81.8	Chalk	68.8	Chalk
Layer 12	74	65	Tor	500.7	Chalk	191.4	Chalk
Layer 13	93.5	74	Hod	524.2	Chalk	185.4	Chalk
Layer 14	98.9	93.5	Herring				
Layer 15	105	99.5	Roedby–Plennus Marl				
Layer 16	127	105	Britannia				
Layer 17	136.5	127	Valhall	85.7	30% sst; 70% shale	15.1	30% sst; 70% shale

Table 2. Continued

(C)

Layer	Start Time (Ma)	End Time (Ma)	Formation	Thickness (m) and Lithology (%)**			
				30/2C-4		30/7a-7	
Layer 18	140	136.5	Kimmeridge 1				
Layer 19	142	140	Kimmeridge 2				
Layer 20	150.7	142	Fulmar				
Layer 21	154	150.7	Pentland				
Layer 22	162	154	Brent				
Layer 23	205.7	180	Unconformity				
Layer 24	209.6	205.7	Missing				
Layer 25	211	209.6	Joshua				
Layer 26	214	211	Josephine				
Layer 27	220.7	214	Jonathan			48.6	70% shale; 30% halite
Layer 28	234.3	220.7	Joanne	395.7	70% sst; 30% shale	464.2	50% sst; 30% shale; 10% halite
Layer 29	237	234.3	Julius		80% shale; 20% halite	138.2	80% shale; 20% halite
Layer 30	241.7	237	Judy		70% sst; 30% shale	300	70% sst; 30% shale; 10% halite
Layer 31	251.2	241.7	Smith Bank		80% shale; 20% halite	200	80% shale; 20% halite
Layer 32	259	251.2	Turbot Anhydrite		Halite		Halite

*(A) Values of initial porosity, φo, and constant, A, in the porosity-effective stress relationships of the form $\varphi = \varphi_o e^{-A\sigma v'}$ for the Skagerrak sandstones of channel and sheetflood facies, shale, chalk, and salts, where φ is porosity and $\sigma_{v'}$ is vertical effective stress in megapascals. (B) Constants A and B obtained for vertical permeability-porosity relationships of the form $\log k = A\varphi + B$, where k is vertical permeability in millidarcies. (C) Age, thickness, and lithology content of sedimentary sections for one-dimensional basin modeling of wells 30/2C-4 and 30/7a-7.

**sst = sandstone.

2008). However, we suggest that calculated paleo–pore pressures during the pre-Cretaceous phases of Triassic reservoir development, before any gas generation, were important factor in the maintenance of high primary porosity.

One-Dimensional Model Construction

One-dimensional modeling of nine wells in the J Block (Table 1) was undertaken using TEMISpack v. 2010. The software uses forward modeling and incorporates heat and pressure transfer through time, and calculates mechanical and chemical compaction effects. Seven types of lithology, clays and shale, silty clays, Tertiary and Paleocene sands and sandstones, Jurassic and Triassic sandstones, reservoir chalks, non-reservoir chalks, and salts, were used to model the sediments in the study area. Each interval was assigned suitable geologic parameters (Table 2).

Empirical relationships between porosity and vertical effective stress for the Skagerrak sandstones were derived from downhole density logs and measured pore pressures from modular formation dynamics tester and drill stem test tests. Results from routine core samples analysis were used to construct an empirical relationship between porosity and permeability for the Skagerrak sandstones. Relationships between porosity and vertical effective stress and between porosity and permeability for each

Table 3. Summary of Overpressure Results Obtained from One-Dimensional Modeling of Nine Wells in the North Sea Central Graben, With and Without Syndepositional Halite*

Age	Depth to Top (mbsf)	Overpressure Without the Existence of Halite Cement (MPa)	Overpressure With the Existence of Halite Cements (MPa)
Late Triassic	700–1000	0.3–1.0	2.0–3.0
Late Cretaceous	1300–1500	0.5–1.0	2.7–5.0
Eocene–Oligocene	2000–2200	3.7–7.0	5.0–10.0
Mid-Pliocene–Present day	3000–3500	15.0–18.0	17.0–21.0

*The value ranges given are the modeled values at the end of each of the four phases of overpressure buildup.

lithology are presented in Table 2. For clays and shale, and for Tertiary and Paleocene sandstones, the relationships were empirically constructed based on data from sections where the pore pressure is hydrostatic, or near hydrostatic. The relationship between porosity and vertical effective stress for the chalk given by Lubanzadio et al. (2002) and the relationship between porosity and permeability for nonreservoir chalk given by Megson and Hardman (2001) and Mallon and Swarbrick (2008) were used. For salt, the initial porosity has been estimated to be 0.14% (e.g., Cardell et al., 2002). A slightly higher value of 0.5% was arbitrarily chosen for modeling to avoid exaggeration of its sealing properties.

Other physical properties required for the basin modeling were grain density, matrix thermal conductivity, and heat capacity for each lithology. These data were estimated from core sample analysis and published results (Midttømme et al., 1998). The geologic model for each well was made up of 22 to 28 layers, depending on the stratigraphy. The ages of the layer tops were estimated from the known ages of the key formations (Table 2C).

Paleo-Temperature and Pore-Pressure Reconstruction

Thermal history modeling is essential for paleo–heat flow calibration of the one-dimensional models used as a function of burial history. Several heat flow histories of the Central Graben and, more specifically, of UK Quad 30 in the central North Sea have been published (Swarbrick et al., 2000; Carr, 2003; Primio and Neumann, 2008).

Carr (2003) stated that heat flow from the basement must increase during uplift and decrease during subsidence. Correlating to the tectonic history of the study area, a heat-flow history was constructed based on a two-phase model of rifting (Permian-Triassic to Early Triassic, and Middle to Late Jurassic) and subsidence (Middle Triassic to Middle Jurassic, and Late Jurassic to Holocene). Present-day heat-flow from the basement in the study area is approximately 62 mW/m^2 (Carr, 2003; Primian and Neumann, 2008). Two heat-flow peaks of approximately 95 mW/m^2 associated with the North Sea rifting phases at 240 Ma and 160 Ma were included. Vitrinite reflectance data, maximum temperatures obtained from apatite fission-track analysis, paleotemperatures and paleo–pore pressures obtained from fluid inclusions in mineral cements (Swarbrick et al., 2000; Primio and Neumann, 2008), and new temperature data from recently drilled wells in the study area were used to calibrate the model. We also used published surface-temperature history indications. Paleo–heat flows and paleo–pore pressure were adjusted by trial and error to obtain reasonable agreement between simulated and measured vitrinite reflectance, and values of paleotemperature and paleo–pore pressure (Swarbrick et al., 2000; Primio and Neumann, 2008).

The results of pore-pressure estimation from one-dimensional modeling are summarized in Table 3. Figure 5A and B show burial history and vertical effective stress and overpressure evolution at well 30/7a-9. Pore pressures in the Skagerrak Formation are at their maximum at the present day. The Skagerrak Formation in the Central Graben is at its maximum depth of burial at the present day, and

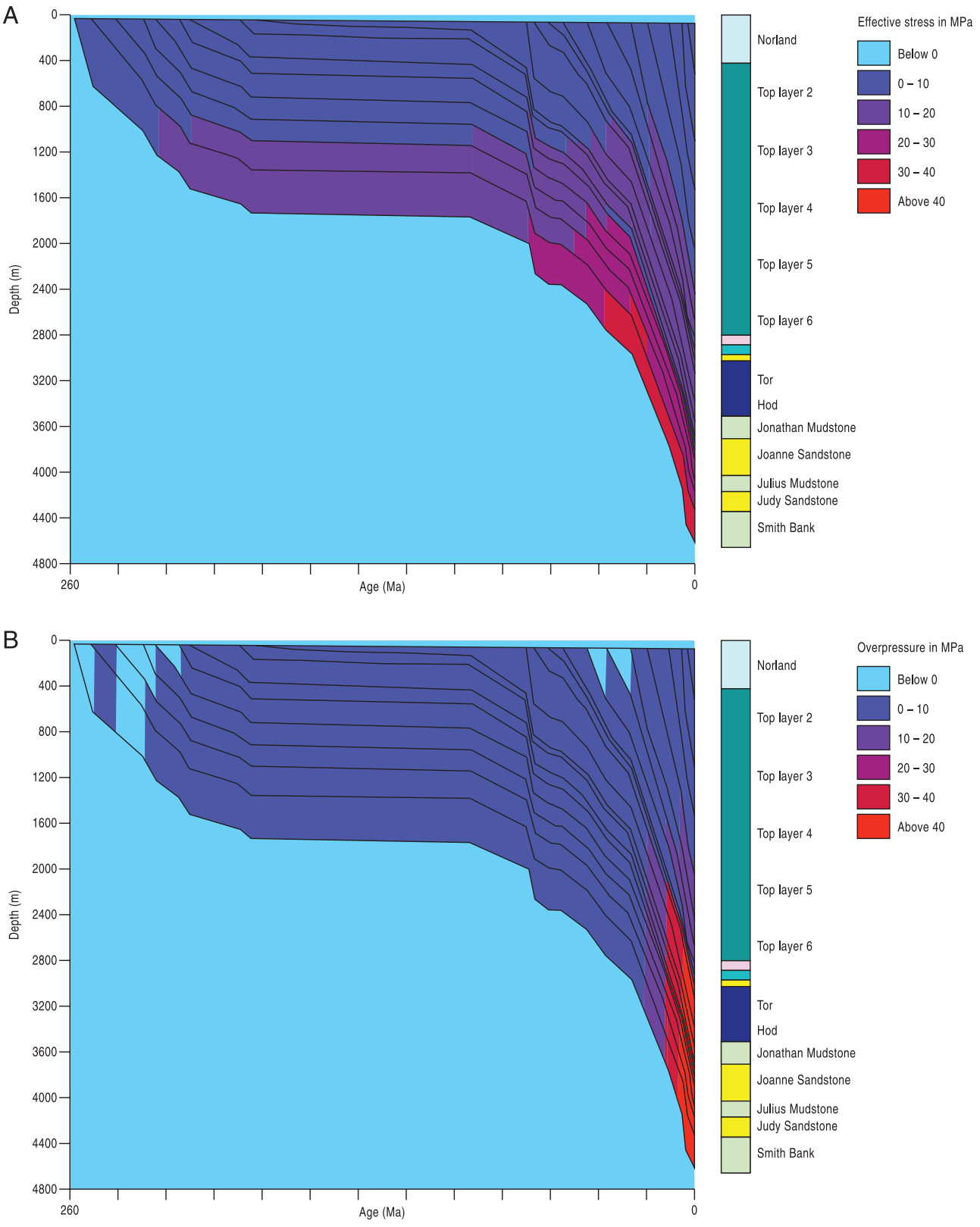

Figure 5. (A) Result from one-dimensional basin modeling at well 30/7a-9: burial history and effective stress evolution. (B) Burial history and overpressure evolution at well 30/7a-7.

modeling results suggest that it experienced maximum vertical effective stress in the early Eocene.

Previous studies of overpressure generating mechanisms in the Triassic Skagerrak Formation identified that pore pressure in the reservoir increased above hydrostatic levels by approximately 10 MPa (1450 psi) at 70 Ma and increased more or less continuously to present-day overpressures of approximately 40 MPa (5802 psi) (Primio and Neumann, 2008). However, the one-dimensional modeling undertaken in this study, supported by data from petrographic observations and laboratory measurements on the Skagerrak mudstone and sandstone members, suggests that overpressures in the J Block Skagerrak Formation were generated during four phases—in the Late Triassic, in the Late Cretaceous, from the Eocene into the Oligocene, and from the mid-Pliocene to the present—when Skagerrak reservoirs experienced reduced vertical effective stress. Early overpressure was retained during the Late Triassic because of the sealing properties of the intercalated mudstone members in the Skagerrak Formation, which contained syndepositional evaporites. Overpressure in early burial history was probably important in restricting fluid flow and quartz cementation and will be discussed further below.

PETROGRAPHIC METHODS AND DATA COLLECTED

Nine wells were chosen from 3400 to 5020 m (11,155–16,470 ft) below seafloor covering the main sedimentary facies within the Judy and Joanne Sandstone Members of the Skagerrak Formation, as previously described (Table 1). The samples were all within the temperature range of 130°C to 180°C, effective stress range of 10 to 21 MPa (1450–3046 psi), and overpressure range of 22 to 40 MPa (3191–5802 psi). All the wells studied had continuous core through the main sandstone members. One-hundred thin sections and 117 bulk rock specimens from representative sections of each well were studied.

Porosity in the thin sections was identified using blue epoxy resin impregnation under vacuum, and potassium feldspars were stained yellow using sodium cobaltinitrite. Modal analysis was conducted by point counting with 300 counts per thin section. The resulting data were used to identify and quantify depositional and diagenetic reservoir quality trends and to select samples for additional analyses.

All the thin sections were highly polished (30 nm) before examination with a Hitachi TM 1000 scanning electron microscope (SEM) and a Hitachi SU-70 field emission gun, both equipped with an energy-dispersive detector (EDS). Scanning electron microscope analyses of thin section and bulk rock samples were conducted at 15 to 20 kV acceleration voltage with beam currents of 1 and 0.6 nA, respectively. To take SEM images using the Hitachi SU-70 field emission gun, bulk rock samples and thin sections were prepared without coverslips and were carbon coated. Point analyses had an average duration of 2 min, whereas line analyses were dependent on length. Scanning electron microscope–EDS was used for rapid identification of chemical species and orientation on the sample. A Gatan monocathodoluminescence monochromator was used to characterize different cement generations and to interpret the origin of detrital quartz grains. Additional data, such as clay mineral content obtained from x-ray diffraction, fluid inclusion, porosity, permeability, bulk density, and grain density data were included for all wells in this study.

PETROGRAPHY RESULTS

The present-day Skagerrak fluvial reservoir quality is the cumulative expression of several depositional attributes (e.g., facies architecture, grain composition, sorting, and size), acted on by early diagenesis and, subsequently, by other diagenetic events during continued burial and later tectonics.

Depositional Controls On Reservoir Quality

In the Triassic, the study area lay at the distal end of an ephemeral fluvial and lacustrine system that was sourced mostly from the north, with deposition commencing during the Middle Triassic (Anisian) and terminating during the Late Triassic (Rhaetian)

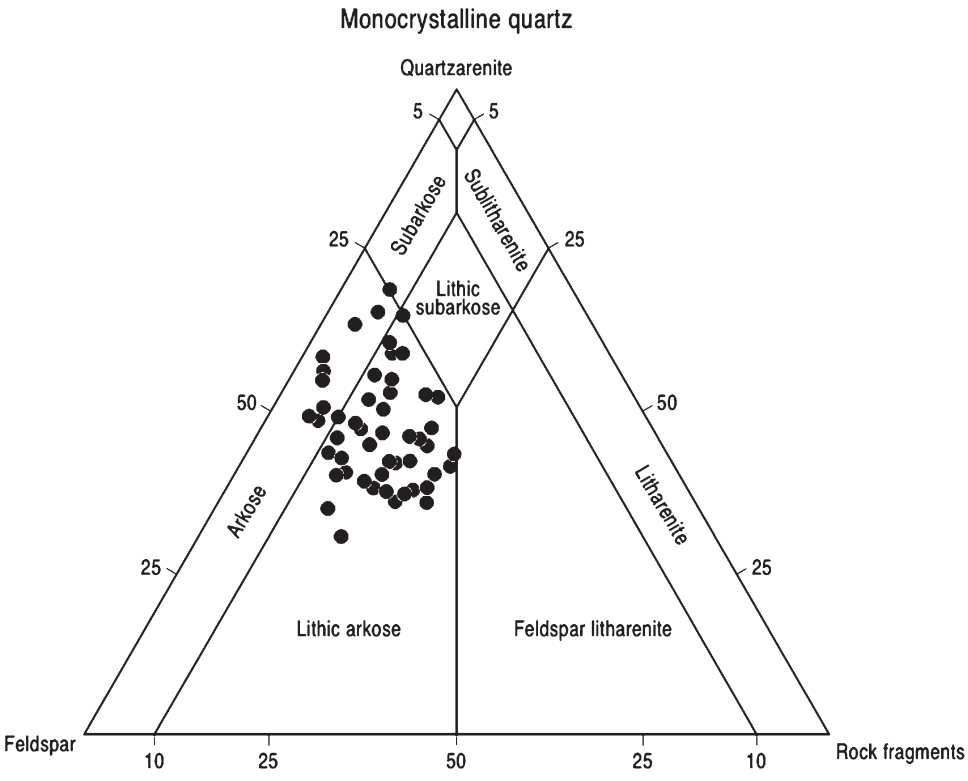

Figure 6. Classification of the Triassic Skagerrak sandstones found in J Block, United Kingdom quad 30.

(Goldsmith et al., 1995, 2003; McKie and Audretsch, 2005). The Skagerrak Formation consists of three thick sandstones (Judy, Joanne, and Josephine Members) and thin, interbedded gray and red mudstones that were deposited in a channelized and sheetflood fluvial environment. The sandstone deposition was interspersed by predominantly mudstone units (Julius, Jonathan, and Joshua Members) deposited in ephemeral playa lakes, with some marginal lacustrine deposition (Figure 3).

The depositional facies of the Skagerrak Formation have been described by several previous authors (e.g., Hodgson et al., 1992; Goldsmith et al., 1995, 2003; Fisher and Mudge, 1998; Keller et al., 2005; McKie and Audretsch, 2005; Archer et al., 2010; McKie et al., 2010). The fluvial sandstone reservoir facies include confined, channelized and unconfined, sheetflood, and crevasse splay components (N. Meadows, 2011, personal communication). Mudstones and siltstones constitute the nonreservoir floodplain and playa facies. Paleosols occur in all the facies, commonly as rip-up clasts within the base of the fluvial channels.

The Skagerrak reservoir channel sandstones cover a narrow range of compositions. Most are arkosic to lithic-arkosic arenites (Figure 6). Average grain size and sorting for the J Block study area wells are shown in Table 4. Interestingly, grain-size variability is limited across all facies, with most of the sands being fine and very fine grained with a mean grain size of 0.05 to 0.15 mm (0.002–0.006 in.). Coarser grain sizes are encountered within the lower parts of the confined channelized sands, with a mean grain size of 0.35 mm (0.014 in.) (medium grain size). Point counting and digital image analysis technique using jPOR, to quantify porosity and pore diameters, was used (see Grove and Jerram, 2011). Pore diameter values over the range of 0.03 to 0.15 mm (0.001–0.006 in.) were measured (Figure 7) and are micropores (0.01–0.1 mm [0.0004–0.004 in.]) according to the classification scheme proposed by Katsube et al. (1999a, b). In some samples, pores are bigger than the surrounding grains identified using whole-rock samples in the SEM.

The mean pore size of channelized sands is approximately 0.06 mm (0.002 in.), with 50% of the pores larger than the mean value and 8% to 10% of the pores greater than 0.1 mm (0.004 in.) in diameter (Figure 8) (Table 4). The mean pore

Table 4. Grain Size, Pore Size, and Other Measured Parameters for the Skagerrak Joanne and Judy Sandstones in J Block, United Kingdom Quad 30

					Grain Size (0.25 μm)			Pore size (0.25 μm)			Grain Contact		Grain Contact Volume	Grain Volume	Porosity	Total Cement		
No.	Well	Sample Number	Depth (mbsf)	Member	Median	Arithmetic Mean	Standard Deviation	Median	Arithmetic Mean	Standard Deviation	Point Contact (%)	Line Contact (%)	(%)	(%)	(%)	(%)	CoPL*	CePL*
1	30-2C-4	S50	3593.6	Joanne	55	55	19.2	23.5	25.2	7.3	32	68	12.7	64.5	20.9	1.9	28.8	1.4
2	30-2C-4	1RR	3630.5	Joanne	61.6	67.1	26.7	35.7	42.9	22.5	36.6	63.4	6.1	57.9	30.6	5.4	14.1	4.6
3	30-2C-4	S24	3506	Joanne	58.7	65	29.1	35.7	42.7	23.1	36.6	63.4	9.6	61.1	25.7	3.6	22.2	2.8
4	30-2C-4	S42	3544.1	Joanne	60.7	66	28.3	32.3	37.1	16.1	40.2	59.8	5.5	54.1	30.3	10.1	7.7	9.3
5	30-2C-4	S15	3979.8	Judy	61.7	67.7	27.1	32.5	37.8	18.3	33.8	66.2	7.9	60	29.6	2.5	19	2
6	30-2C-4	S18	3984.5	Judy	66.3	70.7	27.4	34.3	37.7	15.6	29.7	70.3	8.7	63.5	25.3	2.5	23.8	1.9
7	30-2C-4	1RR	4760.5	Joanne	68.8	88.5	61.2	65	83.6	57.9	18.8	81.3	2.8	61.2	16.6	19.4	14.1	16.7
8	30-2C-4	2RR	4768.6	Joanne	88.6	92.8	45.9	38.7	51.1	33.8	20.8	79.2	3	62.4	31.4	3.2	15.9	2.7
9	30-2C-4	3RR	4754.9	Joanne	61.6	72.4	38.8	41.6	61.8	49.3	22.1	77.9	3.6	61.9	32.6	1.9	16	1.6
10	30-2C-4	8RR	4804.2	Joanne	59.3	61.5	19.8	39.1	43	17	20.4	79.7	3.2	63.5	30.2	3.1	17.5	2.6
11	30-7a-8	S8	4759.7	Joanne	100	114.7	69	42.5	55.2	33.6	12.5	87.5	3.1	63.7	28.8	4.4	17.7	3.6
12	30-7a-8	S1	4589.4	Joanne	95.8	99.8	38.9	44.1	51.2	23.5	11.1	88.9	4.4	65	28.7	1.9	20.7	1.5
13	30-7a-11z	S13	4782.6	Joanne	100.4	102.9	40.3	43.2	49.7	22.3	11.4	88.6	4.6	64.2	28	3.2	20.1	2.6
14	30-7a-11z	S3	4752.3	Joanne	100.5	106.8	46.3	40.9	47.1	20.8	12.5	87.5	5.4	68.6	23.1	2.9	25.7	2.2
15	30-7a-P3	S16	4785.6	Joanne	79.1	83.6	33.5	38	42.2	15.8	13.1	86.9	5.7	62.1	21.3	10.9	18.9	8.8
16	30-7a-P3	S22	4801.9	Joanne	74.9	83.6	40.6	33.7	36.9	12.7	18.2	81.8	6	66.6	10.2	17.2	24.2	13
17	30-13-5	S1	3943.9	Joanne	56	58.3	17.7	24.4	26.7	9	24.5	75.6	13.5	62.5	18.6	5.4	27.6	3.9
18	30-13-5	S5	3961.2	Joanne	69.7	77.3	34.6	31.3	34.8	13.3	21.7	78.3	9.1	68.4	20.1	2.4	29	1.7
19	30-13-5	S6	3961.6	Joanne	91.8	96.9	42.3	46	53.9	31.1	26.6	73.4	4.7	59.7	29.3	6.3	14.6	5.4
20	30-13-5	S7	3962.3	Joanne	55.4	59.7	23.1	26.9	33.7	19.3	26	74	7.5	52.5	29.5	10.5	8.3	9.6
21	30-13-5	S33	3974.7	Joanne	71.3	78.3	34.2	26.5	30.4	12.9	26.1	73.9	10.7	70	15.7	3.6	31.8	2.5
22	30-13-5	S42	3996.4	Joanne	60.9	65.2	25.4	24.9	27.8	10.3	30	70	11.1	66.2	20.3	2.4	28.8	1.7
23	30-2C-4	4RR	4788.7	Joanne	62.18	71.06	35.24	36.58	49.22	35.56	23.06	76.94	2.9	57.5	35	4.6	8.9	4.2
24	30-2C-4	S11	4773.3	Joanne	90.55	101.53	56.17	39.78	51.16	31.21	17.77	82.23	3.4	60	30.7	5.9	13.2	5.1
25	30-7a-8	2RR	3401.6	Joanne	60.16	64.94	25.46	31.82	38.27	19.53	37.38	62.62	6.4	58.3	33.9	1.4	15	1.2
26	30-7a-8	S29	3561	Joanne	53.62	53.62	29.96	30.86	36.25	17.53	38.12	61.88	7.5	57.2	32.5	2.8	15	2.4
27	30-7a-8	S34	3568.8	Joanne	82.13	82.13	46.33	40.65	48.95	27.63	24.01	75.99	6.7	65.5	23.6	4.2	23.8	3.2
28	30-7a-8	7RR	3401.6	Joanne	60.16	64.94	25.46	31.81	38.27	19.53	37.38	62.62	6.4	58.3	33.9	1.4	15	1.2
29	30-7a-9	4RR	3691.1	Joanne	87.45	95	42.95	43.79	49.15	22.24	26.01	73.99	5.2	63.9	26.8	4.1	20.4	3.3
30	30-7a-9	5RR	3681.1	Joanne	85.91	93.82	43.31	46.37	53.3	26.73	28.8	71.2	4.6	61	30.9	3.5	16.2	2.9
31	30-7a-9	7RR	3708.5	Joanne	82.37	95.41	50.06	38.15	47.82	28.58	22.19	77.81	6.4	66.6	23	4	24.7	3
32	30-7a-11z	S35	3530.5	Joanne	58.48	63.35	24.68	30.25	34.18	14.92	31.94	68.06	5.9	59.2	31.7	3.2	15.5	2.7
33	30-7a-P3	S2	3948.5	Judy	56.36	70.41	42.72	24.75	34.29	26.89	37.84	62.16	5.4	54.4	29.8	10.4	8	9.6
34	30-7a-P3	S13	3976.7	Judy	68.44	78.53	40.32	36.97	43.74	23.44	32.72	67.28	6.3	61	27.1	5.6	18.3	4.6
35	30-13-5	S2C	3955.9	Joanne	53.57	54.71	14.17	24.27	25.13	5.33	29.36	70.64	13.6	59.3	21	6.1	24.6	4.6

36	30-13-5	S15	3958.8	Joanne	112.28	118.82	58.23	47.41	53.55	24.74	20.09	79.91	5.1	67.8	21.9	5.2	24.6	3.9
37	30-13-5	S8C	3962.8	Joanne	69.03	73.64	29.02	24.82	25.98	6.6	26.02	73.98	11	66.1	14.3	8.6	28.7	6.1
38	30-13-5	S8	3962.8	Joanne	69.77	70.79	19.68	22.52	24.37	7.7	25.49	74.51	15.7	62.7	10.3	11.3	29.8	7.9
39	30-13-5	S9	3964.7	Joanne	83.35	90.66	39.65	37.73	42.43	18.33	16.1	83.9	8	68.6	20.3	3.1	28.2	2.2
40	30-13-5	S40	3989.7	Joanne	65.49	75.11	36.95	28.99	32.76	13.07	32	68	8.5	68.1	20	3.4	28.2	2.4
41	30-2C-4	5RR	4783.2	Joanne	54.83	60.19	23.43	40.47	48.37	25.12	23.92	76.08	1.6	54	14.2	30.2	1.1	29.9
42	30-2C-4	6RR	4789	Joanne	57.75	63.36	26.47	39.69	49.17	28.24	18.12	81.88	1.4	54.5	20.2	23.9	1.6	23.5
43	30-13-5	S3	3959.6	Joanne	ND**	ND	ND	ND	ND	ND	ND	ND	ND	ND	ND	ND	ND	ND
44	30-7a-8	3RR	3602.7	Joanne		94	49.9	49.2	57	29.4	26	74	4	57.7	22.7	15.6	10.9	13.9
45	30-7a-8	4RR	3596	Joanne		71.6	36.9	46	54	29	23.3	76.7	5.6	56.4	19.6	18.4	11.3	16.3
46	30-7a-8	5RR	3585.4	Joanne		67.5	30.7	45.3	50.3	22.4	23.3	76.7	6.1	56.1	19.9	17.9	11.6	15.8
47	30-7a-8	6RR	3575.6	Joanne		61.7	31	41.2	48.5	25.6	18.1	81.9	6.5	57.2	21.2	15.1	13.7	13
48	30-7a-8	7RR	3562.5	Joanne		64.3	31.8	29.6	35.5	17.7	34.8	65.3	7.8	59.5	27	5.7	18.3	4.7
49	30-7a-8	8RR	3619.5	Joanne		99.7	54.3	34.3	43.5	26.4	39.4	60.6	5.5	68	24	2.5	25.2	1.9
50	30-7a-8	1RR	3630.5	Joanne		67.1	26.7	35.7	42.9	22.5	36.6	63.4	6.1	57.9	30.6	5.4	14.1	4.6
51	30-7a-8	S31	3563.8	Joanne		49.8	35.1	28.7	36.7	20.9	42.7	57.3	5.8	58.1	31.2	4.9	13.9	4.2
52	30-7a-9	1RR	3674.7	Joanne		79.2	28.6	26.9	27.8	7	36	64	9.3	67	18.9	4.8	27.9	3.5
53	30-7a-9	3RR	3664.9	Joanne		66.9	29.3	27	30.9	12.8	31	69	9.3	64.8	21.1	4.8	25.8	3.6
54	30-7a-9	6RR	3668.1	Joanne		78.1	29.5	21.2	22.3	4.6	20.9	79.1	13.8	71.1	10.1	5	35.2	3.2
55	30-7a-11z	S12	3486.6	Joanne		98.2	43.4	41.8	47.6	22.6	19.1	80.9	6.9	66.9	21.7	4.5	25.5	3.4
56	30-7a-11z	S53	3561.1	Joanne		70	21.9	38.3	42.6	19.8	12.2	87.8	9.9	61	25.7	3.4	22.4	2.6
57	30-7a-P3	S9	3972.5	Judy		64	24	31.3	36.1	16.2	33.2	66.8	8.4	59.7	29.5	2.4	19.2	1.9
58	30-2C-4	S20	4798.2	Joanne		107.7	52.5	43.5	51.5	25.8	11.4	88.6	4.3	65.3	26.5	3.9	21	3.1
59	30-2C-4	7RR	4800	Joanne		69.7	40.2	39.7	49.7	29.2	17.4	82.6	2.6	60.6	17.1	19.7	13	17.1
60	30-2C-4	S27	4813.4	Joanne		152.3	79.9	40.7	47.9	22.9	8.8	91.2	5.4	77.7	13.3	3.6	33.8	2.4
61	30-13-5	S4C	3960.5	Joanne		65.6	18.3	21	22	5	18.3	81.7	6.1	68.4	12.2	13.3	26.2	9.8
62	30-13-5	S10	3965	Joanne		128.6	55.2	49.7	56.4	26.8	17.6	82.5	4	66	24.6	5.4	21.4	4.2
63	30-13-5	S28	3968.8	Joanne		119.3	44.9	42.8	47.5	19.5	12.3	87.7	8	72.5	15.3	4.2		2.9
64	30-7a-7	1RR	3504	Judy	66.6	68.6	24.1	39.1	48.2	25.8	19.4	80.7	4.6	58.4	29.9	7.1	31.7	6.2
65	30-7a-7	4RR	3511.6	Judy	92.7	95.1	31.3	40	44.7	18.2	22.6	77.5	5.2	68.9	22.6	3.3	25.8	2.4
66	30-7a-7	5RR	3488.8	Judy	72.9	74.4	24.8	40.7	47.6	22.8	19.4	80.6	4	64.5	30.6	0.9	19.7	0.7
67	30-7a-7	2RR	3447	Judy	71.1	74.6	26.1	37.9	42.1	17.4	19.8	80.2	6.3	68.9	24.6	0.2	26.9	0.1
68	30-7a-7	3RR	3457.7	Judy	70.9	72.3	23.4	40.9	47.7	22.5	19.3	80.7	4.3	61.5	33.3	0.9	16.4	0.8
69	30-7a-7	S25	3441.1	Judy	86.8	90.3	31	33.1	35.5	11.6	22.7	77.3	10.6	72.4	15.4	1.6	33.7	1.1
70	30-7a-7	S26	3442.7	Judy	86.5	91	32.3	37.7	42.4	19.7	12.7	87.3	6	66	22.2	5.8	23.6	4.4
71	30-7a-7	S31	3449.6	Judy	99.9	105	39.3	35.9	38.2	12.8	24.2	75.8	7.9	67.2	23.6	1.3	26.8	1
72	30-7a-7	S37	3451.9	Judy	75.1	77	25.6	35.9	38.2	12.8	24.2	75.8	7.9	63.8	24.6	3.7	23.3	2.8
73	30-7a-7	S47	3459.9	Judy	76.7	79.9	36.9	28.3	29.4	8.4	22.9	77.1	10.8	64.5	14.8	9.9	27	7.2
74	30-7a-7	S58	3487.7	Judy	84.1	87.6	31.6	31.3	33.7	11.6	18.6	81.4	10.1	72.6	13	4.3	33.5	2.9
75	30-7a-7	S66	3494.6	Judy	66.5	68.6	20.9	31.4	34.6	11.3	10.9	89.1	8.5	67.2	7.7	16.6	27.3	12.1
76	30-7a-7	S71	3506.2	Judy	66.9	72.5	36.1	33	37.9	17.2	22	78	8	58.7	13.9	19.4	17.5	16

Table 4. Continued

No.	Well	Sample Number	Depth (mbsf)	Member	Grain Size (0.25 μm)			Pore size (0.25 μm)			Grain Contact		Grain Contact Volume (%)	Grain Volume (%)	Porosity (%)	Total Cement (%)	CoPL*	CePL*
					Median	Arithmetic Mean	Standard Deviation	Median	Arithmetic Mean	Standard Deviation	Point Contact (%)	Line Contact (%)						
77	30-7a-7	S73	3507.1	Judy	92.1	96.3	32.3	34.2	39.2	18.6	14.8	85.3	7	67.2	12.6	13.2	25.9	9.8
78	30-7a-7	S77	3511.1	Judy	80.3	85.5	33.5	35	37.6	13.1	21.6	78.4	7.5	65	17.8	9.7	24.1	7.4
79	30-7a-7	S82	3516.5	Judy	71	75.2	28.9	34.3	37.5	13.4	24.8	75.2	7.5	63.5	24.3	4.7	22.5	3.6
80	30-7a-8	S24	3553	Joanne	104.6	104.6	49.1	32.7	37.4	16	34.3	65.7	8.6	73.1	17.5	0.8	32.7	0.5
81	30-7a-8	S59	3616.4	Joanne	54.1	54.1	63.1	25.3	27.6	7.7	35.8	64.2	9.5	67.4	22.4	0.7	28.5	0.5
82	30-7a-8	S67	3623	Joanne	49.7	56.6	24	25.9	28.5	10.5	27.1	72.9	9.3	63.5	26.9	0.3	24.5	0.2
83	30-7a-8	S77	3638.3	Joanne	53.7	64.2	34.3	26.2	29.7	12.7	36.5	63.5	8.5	66.4	22.7	2.4	26.6	1.8
84	30-7a-9	2RR	3689.6	Joanne	69.7	72.6	24.8	36.3	42.1	20.2	25.6	74.5	7.3	57	26	9.7	14.5	8.3
85	30-7a-11z	S18	3499.7	Joanne	53.8	55.2	14.7	25.2	27.7	9.3	32.6	67.4	11.1	61.3	25.9	1.7	24	1.3
86	30-7a-P3	S28	4006.7	Judy	69.6	78.4	37.3	36.2	44.3	25.1	32.4	67.6	12.5	61.1	23.6	2.8	25.3	2.1
87	30-7a-P3	S21	3988.4	Judy	54.1	56.9	18.3	25.1	28.5	11	35.4	64.6	6.2	60.2	30.4	3.2	17.2	2.7
88	30-2C-4	9RR	4752.8	Joanne	55.1	58.8	20.8	41.1	46.7	20.3	20.3	79.7	3.3	58.4	15.6	22.7	10.9	20.2
89	30-2C-J7	S7	4983.6	Joanne	82.8	84.7	27.7	38.2	43.1	17.9	14.3	85.7	6	69.5	21.2	3.3	27.2	2.4
90	30-2C-J7	S11	5001.9	Joanne	53.9	56.9	19.1	34.3	39.8	18.4	22.4	77.6	5.1	61	21.7	12.2	16.8	10.2
91	30-2C-J7	S13	5002.3	Joanne	50.7	57.4	25.6	36	41.4	17.9	14	86	5.6	67.1	14.2	13.1	24.3	9.9
92	30-2C-J7	S17	5016.3	Joanne	65.4	68.9	27.2	40.7	45.6	19.1	9.7	90.3	5.5	62.1	18.2	14.2	18.6	11.6
93	30-2C-J7	S19	5019.4	Joanne	66.5	69.2	28.1	39.2	44.2	18.2	9.8	90.2	5.8	67.5	16.8	9.9	25	7.4
94	30-6-7	S1	4789.6	Judy	116.1	133.5	68.5	45.1	54.3	28.9	10	90	3.8	61.5	25.3	9.4	15.8	7.9
95	30-6-7	S4	4812	Judy	67.6	74.7	33.1	48.2	61	38.1	9.3	90.7	2.4	60.2	25.8	11.6	12.1	10.2
96	30-6-7	S7	4818.5	Judy	84.5	89.6	35.9	35.3	40.1	17.3	13.4	86.6	6.2	71.1	12.4	10.3	28.8	7.3
97	30-6-7	S8	4818.5	Judy	73.8	79.7	33.3	35.8	41.7	20.2	23.3	76.7	4	63.4	20.3	12.3	18.4	10
98	30-6-7	S11	4823.9	Judy	83.9	92	42.8	50.3	59.2	32	10	90	2.8	69.4	27	0.8	23.8	0.6
99	30-6-7	S13	4834	Judy	250.3	271.2	129.3	46	50.8	20.2	3.8	96.3	5.5	75.8	10.2	8.5	32.3	5.8
100	30-6-7	S15	4837	Judy	77.7	80.5	25.9	46.9	55.7	29.6	10.5	89.5	2.8	64.4	26	6.8	18.2	5.6

*CoPL and CePL are porosity losses caused by compaction and cementation, respectively.
**ND = no data.

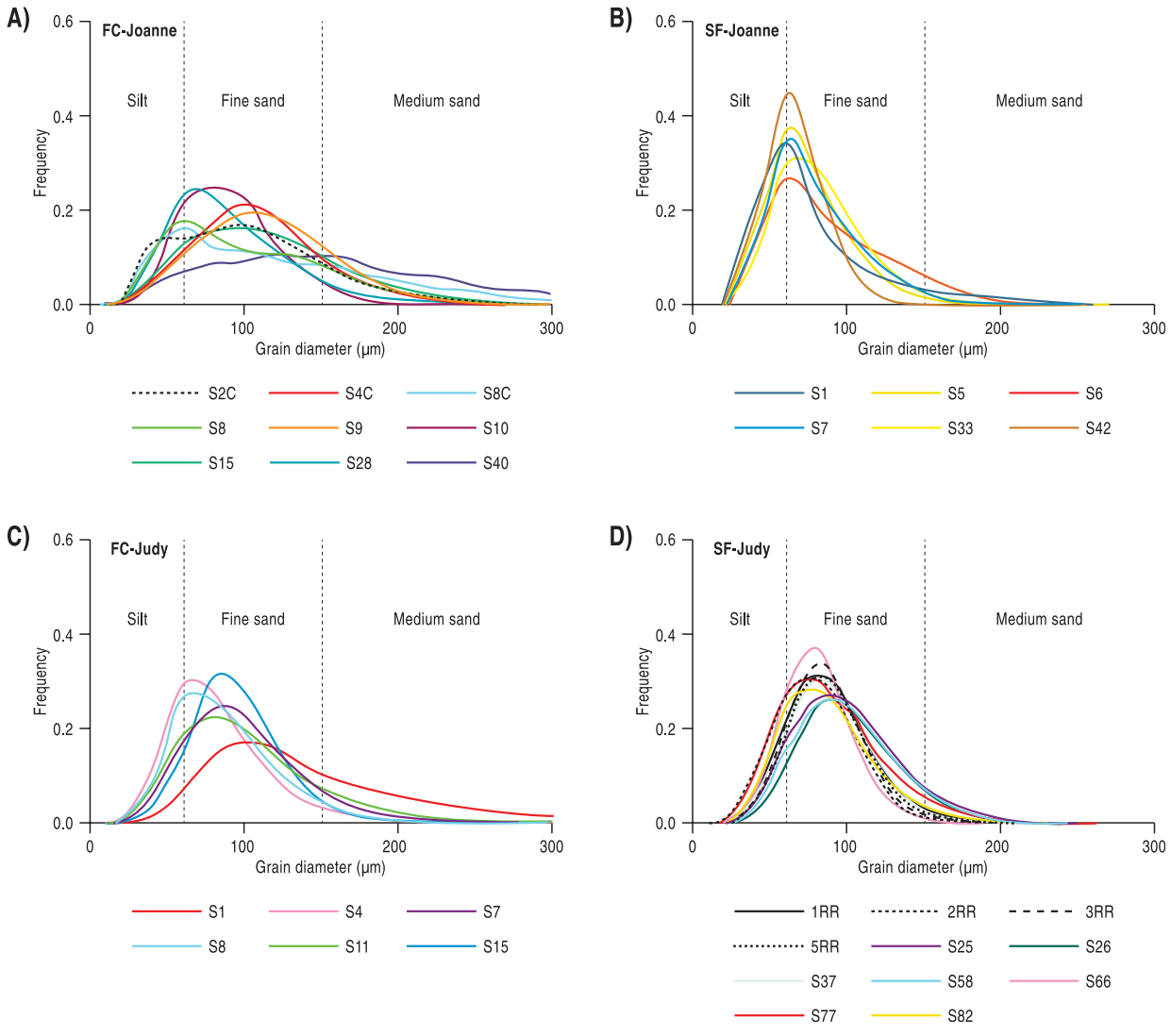

Figure 7. Distribution of grain size of Joanne and Judy Sandstone Members at wells 30/7a-7 and 30/2C-4 for fluvial channel sand facies (FC) and sheetflood facies (SF).

size of sheetflood sands is approximately 0.05 mm (0.002 in.), with 50% of the pores larger than the mean value and 5% to 7% of the pores greater than 0.1 mm (0.004 in.) in diameter. All reservoir channel sandstones are well sorted. Rock texture (grain size and sorting) controls the initial intergranular volume (IGV), porosity, and permeability. Texture is linked to facies through the energy of the depositional environment.

Because the Skagerrak sandstones have undergone minimal pressure dissolution, it is possible to calculate the porosity losses caused by compaction and cementation (CoPL and CePL, respectively; Ehrenberg 1989). An original porosity estimate (OPE) was based on the experimental data of Beard and Weyl (1973) on wet sands and the measured grain size and modal analysis from thin sections. Values of porosity losses caused by compaction and cementation were calculated from the IGV and total cement volumes (CEM):

$$\mathrm{CoPL} = \mathrm{OPE} - \frac{(100 \times \mathrm{IGV}) - (\mathrm{OPE} \times \mathrm{IGV})}{(100 - \mathrm{IGV})} \quad (1)$$

$$\mathrm{CePL} = (\mathrm{OPE} - \mathrm{CoPL}) \times (\mathrm{CEM} \div \mathrm{IGV}) \quad (2)$$

The channelized and confined fluvial components of the Skagerrak sandstones have higher average porosity and permeability compared to the unconfined channels, sheetflood, and crevasse splay

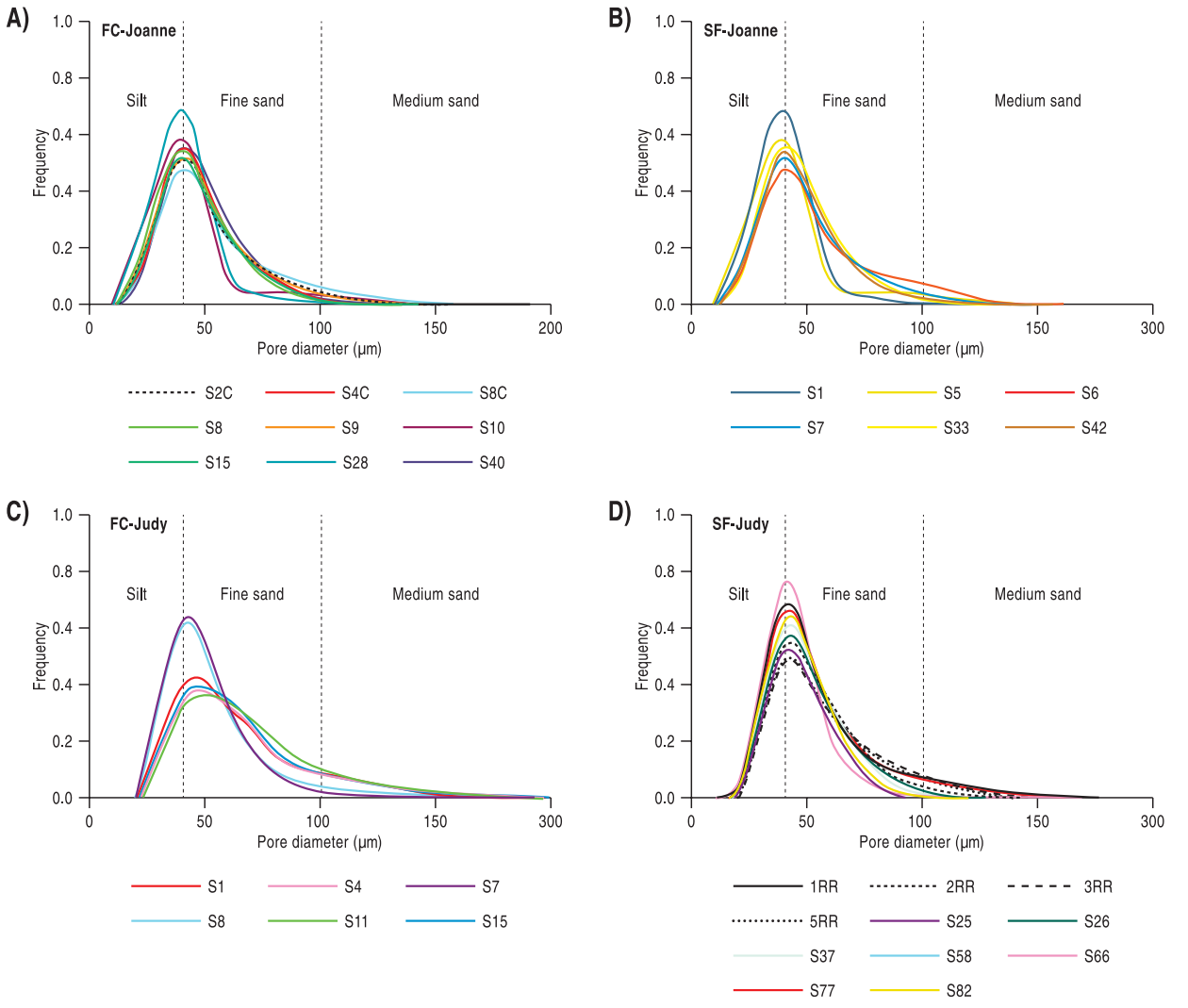

Figure 8. Distribution of pore size of Joanne and Judy Sandstone Members at wells 30/7a-7 and 30/2C-4 for channel sand facies (FC) and sheetflood facies (SF).

components at the present day (Figure 9) (Table 4). The confined channel facies are commonly cleaner sands with a lesser degree of compaction and cementation and can record as much as 35% porosity (Figure 9). Where diagenetic cement is abundant, as in the lower channel parts of several fluvial channels with pedogenic carbonate, differences in reservoir quality between fluvial channel and floodplain facies are nearly obliterated, and reservoir quality is uniformly low.

Diagenetic Controls on Reservoir Quality and Porosity Preservation

A few published studies of the Triassic Skagerrak Formation provide detailed analyses of the diagenesis (e.g., Weibel, 1998, 1999; Swarbrick et al., 2000; Kape et al., 2010). New observations and interpretations relevant to the impact of early diagenesis on reservoir quality and porosity preservation, especially in HPHT provinces, are described here.

Paragenesis of the Skagerrak Formation does not vary significantly within the J Block study area, but some differences do exist with other areas such as the Triassic Skagerrak Heron Cluster, in the northern Central Graben where substantially more chlorite grain coats and pore filling cements commonly occur (McKie and Audretsch, 2005; McKie et al., 2010). Many diagenetic features such as mechanical and chemical compaction, chlorite grain coats, quartz, and halite cements are present throughout, but some minor intrapod and interpod variations

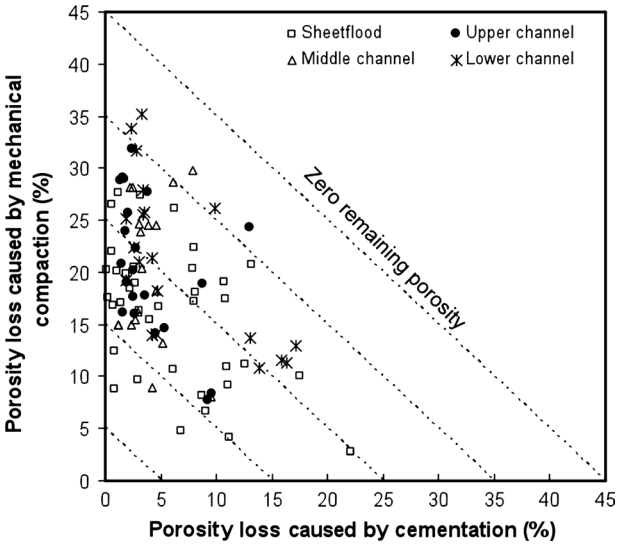

Figure 9. Crossplot showing porosity loss caused by cementation and mechanical compaction for different facies in the Skagerrak Formation.

do occur with dolomite, partially dissolved feldspars, and fibrous pore-lining diagenetic illite. The major cement types important for porosity preservation are illustrated in Figure 10 and are discussed in more detail below.

Quartz Cements

The quartz cements found in the Skagerrak sandstones are microquartz and macroquartz overgrowths (Figure 11). Microquartz is used here as a term for polycrystalline growth patterns of individual micron-size quartz crystals, ranging from 1 to 5 µm in length, which are in optical continuity with the detrital quartz grain (Figure 11A–C). They have variable shapes, but most tend to be elongated to platey in form. Microquartz coatings can be disrupted by any cavities on the detrital grain surface, and the random orientations of the micron-size quartz cystals can interfere with the formation of later quartz overgrowths (Bloch et al., 2002; Taylor et al., 2010). Two discrete phases of microquartz cementation early in the diagenetic history can be seen by SEM-cathodoluminescence (CL) analysis (Figure 11B). This has been further verified using SEM-EDS and the elemental mapping of the quartz cement phases.

The macroquartz in the Skagerrak sandstones is defined as syntaxial quartz overgrowths larger than 20 µm (Figure 11A–D). Macroquartz overgrowths

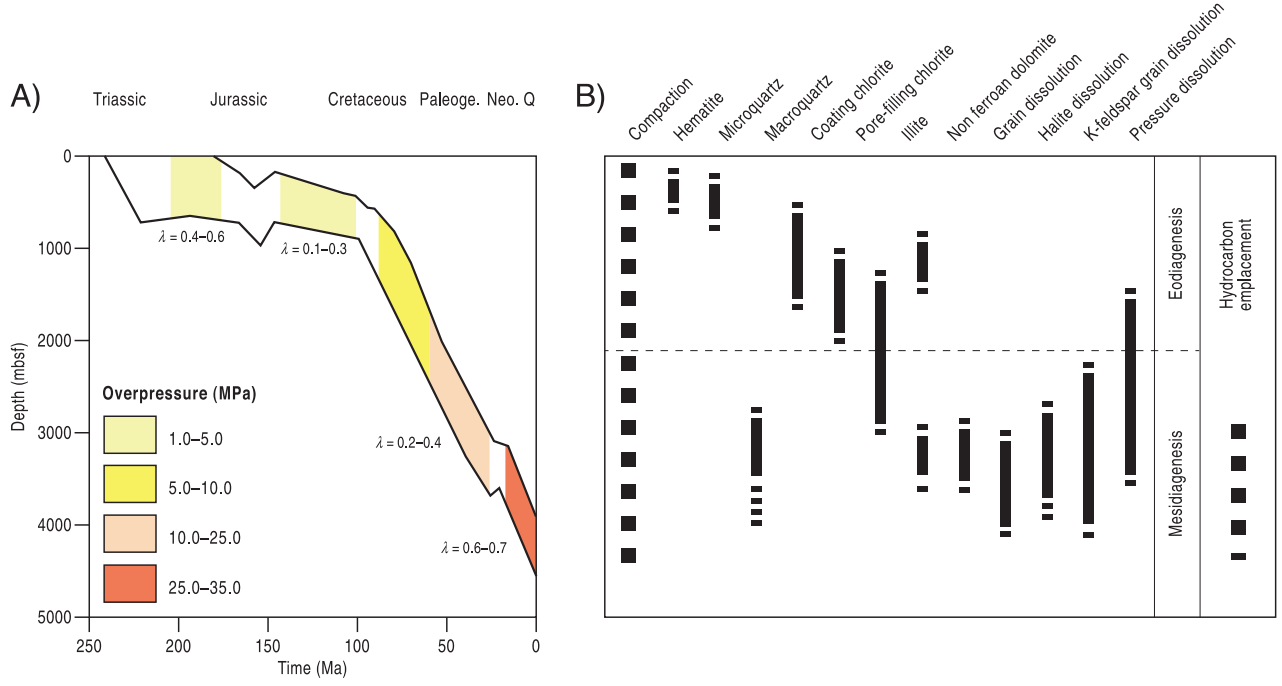

Figure 10. (A) Overpressure history in the Skagerrak Formation estimated from one-dimensional basin modeling of well 30/7a-9. The pore pressure ratio, λ, is defined as $\lambda = (P_p - P_h) / (\sigma_v - P_p)$, where P_p is the pore pressure, P_h is the hydrostatic pressure, and σ_v is the overburden stress. (B) Paragenetic sequence of the main diagenetic processes based on petrographic relationships and basin modeling. Paleoge = Paleogene; Neo = Neogene; Q = Quaternary.

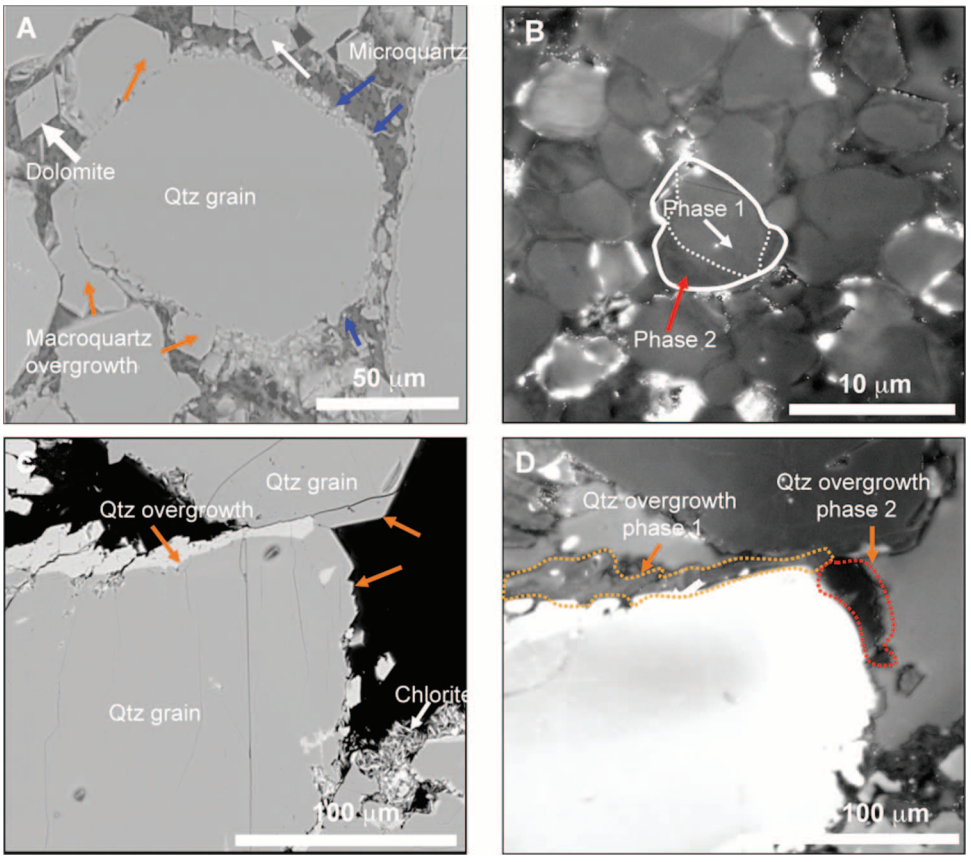

Figure 11. Different types of quartz cement observed in the Skagerrak Formation. (A) Scanning electron microscope image of sample from 4983.6 m (16,350.4 ft) below seafloor in well 30/2C-J7, showing quartz (Qtz) grains, microquartz and macroquartz overgrowths, and sutured grain contacts. (B) Scanning electron microscope image of sample from 3962.3 m (13,000 ft) below seafloor in well 30/13-5 showing different phases of early microquartz. (C) and (D) Scanning electron microscope–cathodoluminescence images of sample from 4812 m (15,787 ft) below seafloor in well 30/6-7 showing different phases of macroquartz overgrowth.

commonly occur in all wells but are particularly common in the deepest wells. In the deepest buried sandstones the macroquartz overgrowths typically occur as two discrete layers as recognized by SEM-CL analysis (Figure 11C). Microquartz coatings can be present beneath the macroquartz overgrowths but are not common.

Sutured quartz-grain contacts are present, typically with chlorite clays occurring on the sutured grain boundaries (Figures 11C, 12). Sutured contacts are also partly evolved between quartz overgrowths and appear to be a late-stage event in the diagenetic history.

Chlorite Cements

Chlorite cement is common in all the Skagerrak sandstones. Chlorite is the most common authigenic clay mineral in the sediments, and it supplies information about the diagenetic history and the chemical composition of pore waters. During diagenesis, the dominant control on the occurrence and type of chlorite is the initial (depositional) mineralogy (e.g., Berger et al., 2009; Dowey et al., 2012). The authigenic chlorite common to all wells, in this study, is magnesium-rich, whereas iron-rich chlorite is more commonly reported in the literature (e.g., Pittman et al., 1992; Bloch et al., 2002; McCartney et al., 2004). Authigenic chlorite is present in three forms:

1. Grain coatings, less than 5 μm thick, covering detrital quartz (Figure 12A) and K-feldspar. Chlorite rims predate the dissolution of K-feldspar and some lithoclasts (Figure 12B). Where chlorite rims are present, the formation of quartz overgrowths were inhibited (Figure 12C).
2. Pore-lining cement, commonly consisting of a thicker rim (~10 μm) covering all detrital grains (Figure 12A, B). Two rim types have been identified in the SEM: an older, poorly crystallized one (type 1 in Figure 12B), and a younger, better crystallized one (type 2 in Figure 12B). The latter consists of subhedral to euhedral,

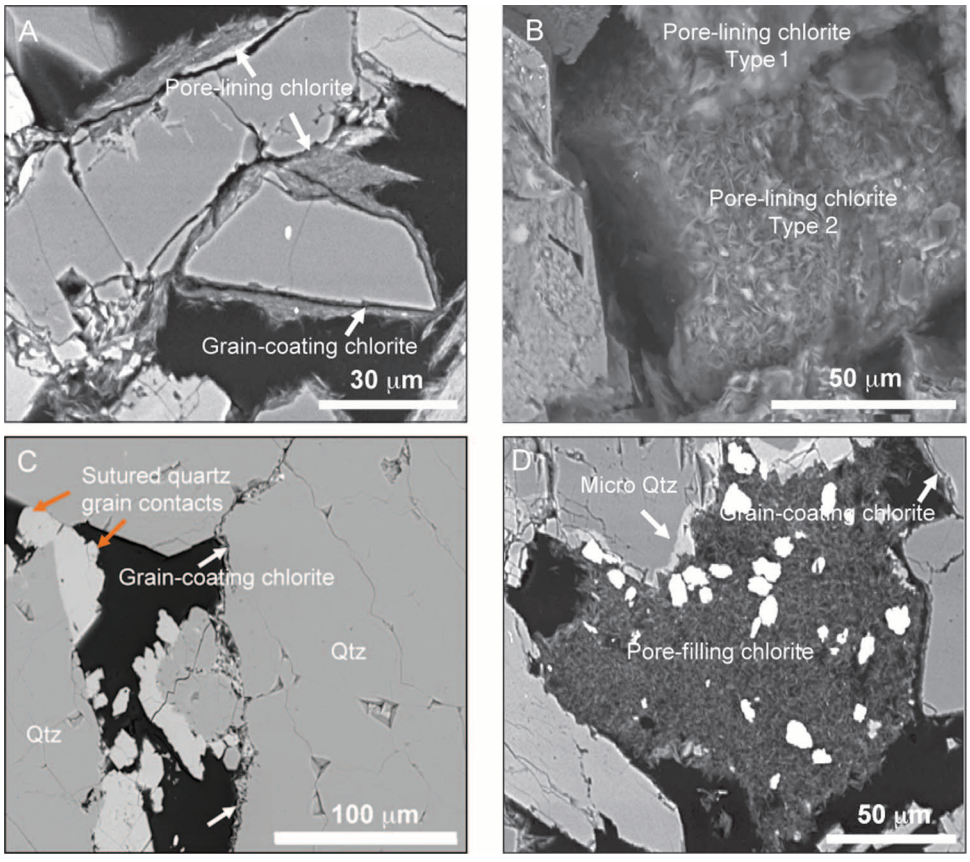

Figure 12. Different types of chlorite observed in scanning electron microscope images of samples from the Skagerrak Formation. (A) Sample from the 3700 m (12,139 ft) below seafloor in well 30/7a-7 showing pore-lining and grain-coating chlorite. (B) Sample from 3506 m (11,503 ft) below seafloor in well 30/7a-7 showing different types of authigenic chlorite found in the Skagerrak Formation. (C) Sample from 4812 m (15,787 ft) below seafloor in well 30/6-7 showing chlorite pore coatings that inhibited macroquartz overgrowth. (D) Sample from 4812 m (15,787 ft) below seafloor in well 30/6-7 showing pore-filling chlorite between grains with microquartz overgrowths and chlorite rims.

pseudohexagonal crystals, oriented with their faces perpendicular to the host detrital grain surface. The underlying older chlorite rim generation is only seen in areas where the younger one has broken away.

3. Pore-filling cements comprise small chlorite plates that are oriented parallel and arranged with a denser packing. Chlorite rims can be covered by pore-filling chlorite cements (Figure 12D).

Authigenic chlorite is the most important and effective grain-coating mineral in terms of limiting early extensive quartz cementation in the Skagerrak sandstones. This is in large part caused by the strong tendency of chlorite to form continuous layers that line the interface between detrital grains and intergranular pore space (Figure 12C). The chlorite forms an important cement in all the Skagerrak sandstones, accounting for as much as 40% and an average of approximately 25% of the total cement. However, it is apparent that, at more than approximately 10% of chlorite, the amount of quartz cementation is greatly reduced (Figure 12C).

Halite Cement

Halite is not commonly reported as a cement nor as a syndepositional aspect in sandstones. The general lack of recognition of halite may partly be caused by its ease of dissolution during water-based coring, slabbing, washing, and standard thin-section preparation. Dissolution can remove halite before sandstone porosity is filled with epoxy for petrographic analysis. The isotropic properties of halite and its low relief in thin section also make it difficult to recognize. Core samples used in this study were cut in oil, and thin sections were prepared in oil-based fluids to preserve any halite cement in the sandstones. Using these precautions, abundant halite has been found as a cement in the Skagerrak sandstones across the J Block and occurs in several forms:

1. Intergranular poikilitic halite cement with euhedral to subhedral crystals of halite 5 to 25 μm in length (Figure 13A, B) is commonly found in macropores. Evidence exists that halite dissolution

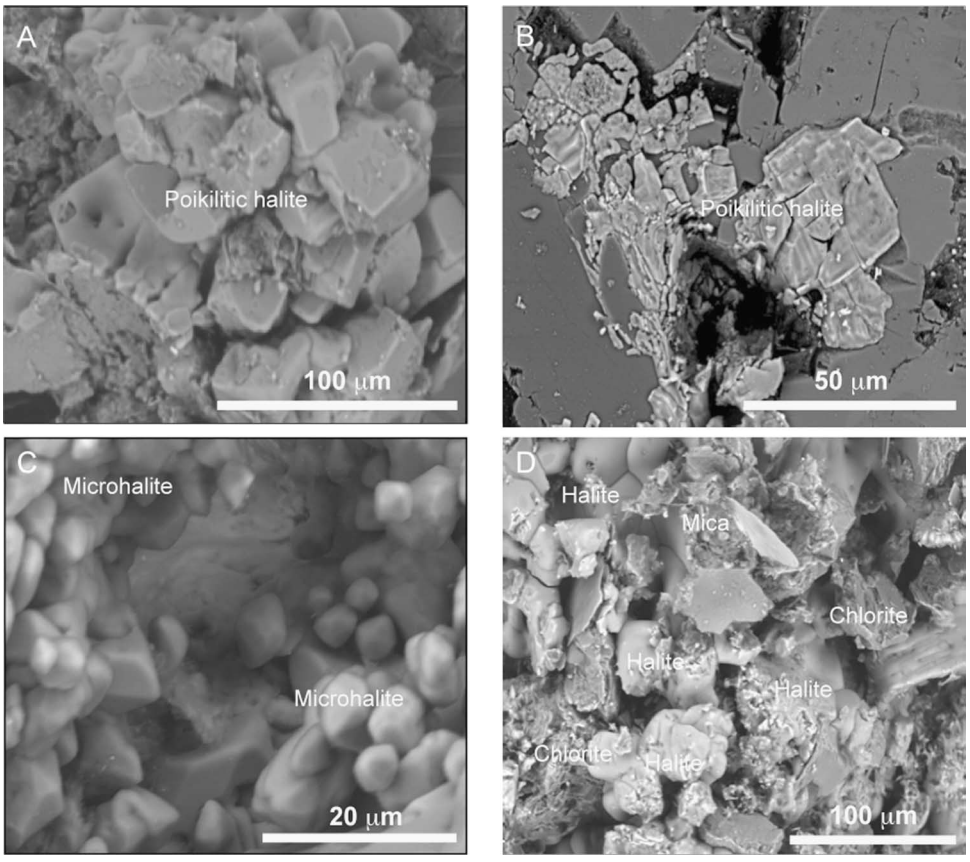

Figure 13. Different types of halite cement observed in scanning electron microscope images of samples from the Skagerrak Formation. (A) Sample from 4773.3 m (15,660.4 ft) below seafloor in well 30/2C-4 showing intergranular poikilitic halite cement. (B) Sample from 3955.1 m (12,976 ft) below seafloor in well 30/13-5 showing poikilitic pore-filling halite. (C) Sample from 4773.3 m (15,660.4 ft) below seafloor in well 30/2C-4 showing microhalite crystals. (D) Sample from 3487 m (11,440 ft) below seafloor in well 30/7a-7 showing halite and chlorite affinity.

has occurred in the macropores: whispers of halite are preserved, and cubic halite pseudomorphs are found around the pore margins.

2. Microhalite cement is identified as polycrystalline micron-size crystals, 1 to 5 μm in length (Figure 13C). Crystals tend to be euhedral to subhedral and are found in direct contact with detrital quartz, K-feldspar grains, and chlorite coats and/or cements.
3. Halite and chlorite show a strong affinity in many wells at all depths in the Skagerrak sandstones. Chlorite plates interleaved with halite are commonly found (Figure 13D). The halite commonly consists of clusters of cubic microcrystalline forms.

INTEGRATED INTERPRETATION

Timing of Diagenetic Processes and Implications

All the diagenetic components of the Triassic Skagerrak Formation sandstones can be linked into a relative sequence of events (Figure 10). After an initial phase of mechanical compaction with a reduction in IGV values, two discrete phases of microquartz coatings were precipitated. These early microquartz coatings, resulting from the rapid crystallization of silica-supersaturated solutions, contributed significantly to the diagenetic transformation of sand to sandstone during the early burial compaction regime. They stiffened the Skagerrak sands early in their burial history, enabling them to maintain high porosity. Recently, empirical evidence from the Middle to Upper Jurassic Brae Formation of the North Sea, United Kingdom, has identified that mechanical compaction halts at the onset of microquartz and quartz cementation with no further change in IGV values (Maast et al., 2011). Furthermore, the occurrence of microcrystalline quartz coatings on detrital quartz grains has been identified as a potentially effective mechanism for inhibiting the formation of pore-filling quartz overgrowths (e.g., Aase et al., 1996). The apparent capacity for microcrystalline quartz to inhibit the development of pore-filling quartz overgrowths is

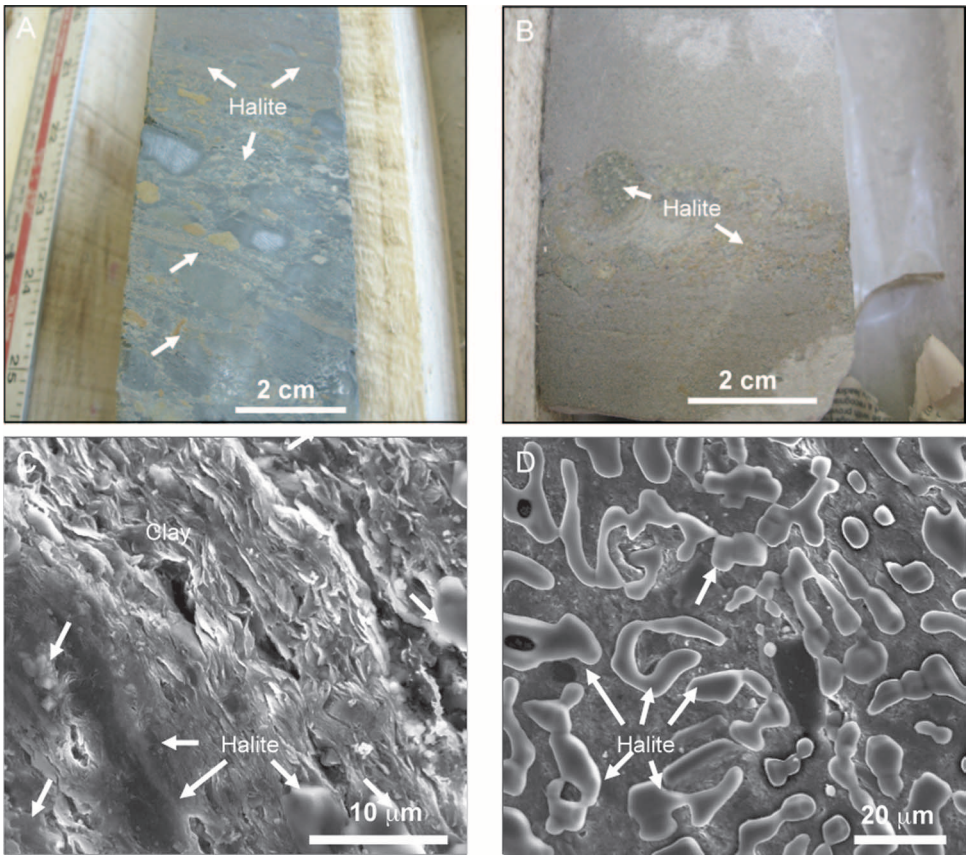

Figure 14. (A) Core photograph of Jonathan mudstone from well 30/7a-7. Syndepositional salts controlled early overpressure development in the Skagerrak Formation. (B) Syndepositional salts are also found in channel sandstones. (C) and (D) High magnification scanning electron microscope images of Jonathan mudstone salts.

likely related to crystal growth mechanics with random *c* axis orientations of microquartz crystals and the different rates of quartz growth on euhedral and noneuhedral quartz surfaces (Haddad et al., 2006; Lander et al., 2008).

The intercalated mudstone members in the Skagerrak Formation (e.g., Jonathan Mudstone Member) (Figure 3) had low permeability at shallow burial because they contain syndepositional evaporites (Figure 14) and hence allowed overpressure to build up early in the burial history during the Late Triassic. The microquartz precipitation probably strengthened the early grain framework and helped inhibit the effects of mechanical compaction (Figures 9, 10). Macroquartz precipitation may also have been inhibited geochemically. Most J Block and central North Sea reservoirs have highly saline pore fluids (Bjørlykke and Gran, 1994; Haszeldene et al., 1999; Wilkinson et al., 2006), and because solubility of quartz decreases with rising salinity, highly saline pore fluids could have inhibited further quartz precipitation from the early stages of burial.

Well-developed chlorite rims and chlorite cements inhibited further secondary quartz cementation on detrital quartz grains (Figure 10). The importance of clay mineral coats, especially chlorite, in preserving porosity has been recognized in many studies (Bloch et al., 2002; Anjos et al., 2003; Berger et al., 2009; Ajdukiewicz et al., 2010; Taylor et al., 2010). Most of the authigenic chlorite coats studied are iron-rich examples and were formed by the reaction of detrital minerals with iron-rich pore waters, the direct replacement of clay precursors such as smectite or kaolinite by chlorite, and neoformation caused by direct precipitation from pore waters (e.g., Anjos et al., 2003). However, in this study, the chlorite coats have been identified as magnesium rich. Kugler and McHugh (1990) recognized that, for the Upper Jurassic Norphlet Formation, Gulf of Mexico, magnesium-rich chlorite coats occur by interaction of precursor clay/iron oxide grain rims with magnesium-rich saline brines derived from underlying evaporites. A parallel can be drawn with the Skagerrak Formation where the simple detrital composition of the Skagerrak sandstones

strongly suggests import of chemical elements from the underlying Permian Zechstein salts and from the syndepositional salt within the Skagerrak mudstone members. Early Mesozoic extension combined with sediment loading contributed to the early mobilization of the Zechstein salt. The deposition of the Skagerrak Formation was confined to minibasins, or pods, flanked by salt walls. Growth of the salt walls and pillows during the Triassic deposition led to a broadening of early minibasins and occurred during the deposition of the Joanne Sandstone Member of the Skagerrak Formation (Davison et al., 2000). Saline pore waters have been widely reported for the central North Sea (usually deeper than 2200 m [7218 ft]) where underlying evaporites are known (e.g., Burley et al., 1989; Bjørlykke and Gran, 1994; McCartney et al., 2004). The magnesium-rich chlorite coats and cements developed as a result of cross-formational flow from Zechstein evaporites and influenced diagenetic reactions from an early stage of burial (Warren et al., 1994). This is demonstrated by magnesium-rich chlorite coatings of channel facies sandstones that commonly have porosities exceeding 25%, and much less quartz than other facies, at depths greater than 4000 m (13,123 ft).

The intergranular poikilitic and microcrystalline halite cements are interpreted to have filled much of the remaining pore space and precipitated directly from the highly saline brines. The charge of basinal fluids saturated with respect to halite must have entered the Skagerrak sandstones early in the burial history, and the halite cements are found associated with chlorite (Figure 10).

K-feldspar detrital grains are present throughout all the wells used in this study, but dissolution is only recognized in samples from depths greater than 3200 m (10,499 ft). The dissolution of K-feldspar commonly results in the formation of late-stage illite where the dissolution of K-feldspar serves as a potassium source to convert kaolinite to illite (Bjørlykke and Aagaard, 1992; Thyne et al., 2001; Peltonen et al., 2009) (Figure 14A, B). However, the low amount (<1%) of illite within the samples is likely to be a consequence of the limited occurrence of kaolinite and high-salinity pore fluids (Gaupp et al., 1993) (Figure 14A, B). At depths greater than 4000 m (13,123 ft), K-feldspar dissolution is important for providing secondary porosity of as much as approximately 5%.

Late-stage dolomite occurs in most samples that were examined (Figures 10, 11A). The ferroan dolomite occurs as pore-filling microcrystalline rhombs, indicating precipitation in reducing conditions. The magnesium for the dolomite precipitation may have been derived from clay mineral transformations (smectite-illite) and at the time of hydrocarbon emplacement (Hendry et al., 2000) or, more likely, from the magnesium-rich saline brines.

Importance of Syndepositional Evaporites in Mudstone and Halite Cements in Sandstone

The recognition of syndepositional evaporites in the mudstones and halite cements in the Skagerrak fluvial sandstones is an important new finding from this research. Syndepositional halite reduced the permeability of Skagerrak mudstone members (Figure 14) and contributed to overpressure retention by disequilibrium compaction. In Table 3, we show the results obtained from our simulations for mudstones with and without syndepositional evaporites. The latter case gave overpressure values much higher than those in the former case. The saline fluids required to form the halite cements in the Skagerrak sandstones of the J Block study area came from the underlying Permian Zechstein and the interbedded mudstone members of the Skagerrak Formation (Figures 3, 14).

Several studies of sandstone reservoirs closely associated with thick salt sections have documented the occurrence of halite cements (e.g., Dixon et al., 1989; Laier and Nielsen, 1989; Purvis 1992; Gluyas and Cade 1997; Weibel and Friis, 2004). In these studies, the halite cement is recorded as late stage and indicates rapid deterioration of reservoir quality through porosity loss. In comparison, the large poikilitic crystal texture and artifacts of pore-filling halite in the Skagerrak sandstones suggest slow crystal growth in sustained phreatic conditions. Furthermore, the different phases of halite associated with chlorite (Figure 13D) indicate that the pore-filling brines were recharged during burial diagenesis.

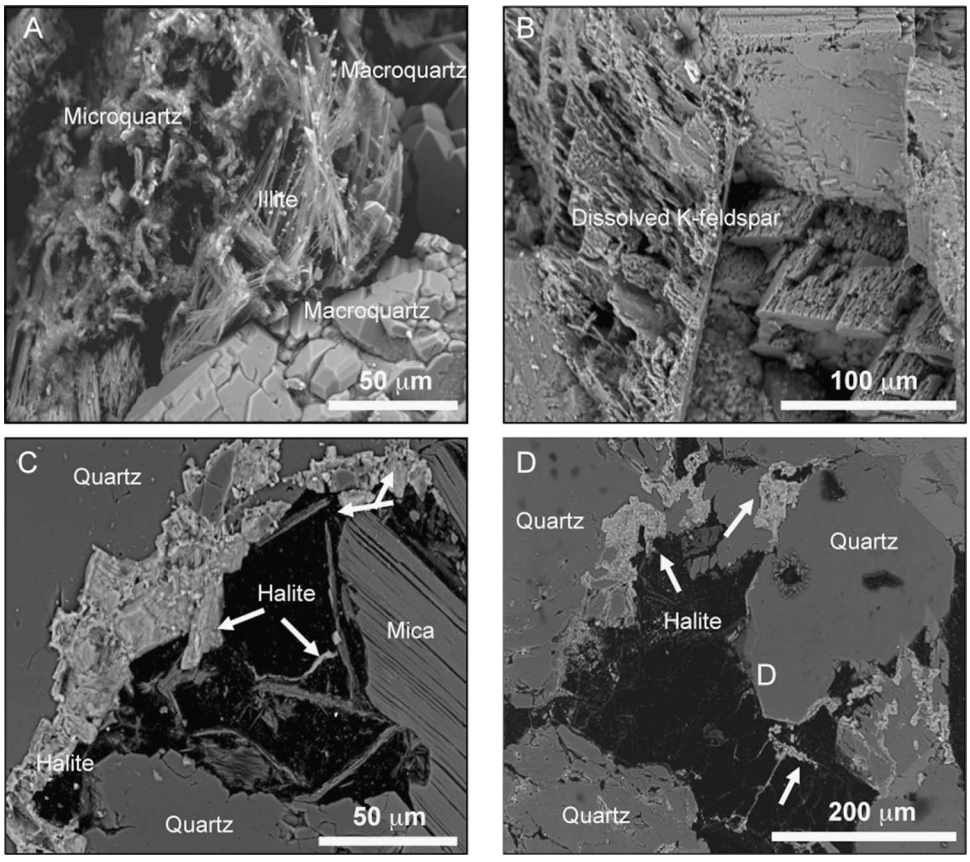

Figure 15. (A) and (B) K-feldspar dissolution with less than 1% illite found in association and secondary porosity development as much as approximately 5%. (C) and (D) Halite cements around margins of pore space in a channel sandstone sample from the 3638.3 m (12,084 ft) below seafloor in well 30/7a-8. Images demonstrate the occurrences of macropores that give rise to porosity of as much as 35%.

Halite pore-filling cements removed most of the remaining porosity in the Skagerrak sandstones, which could have limited the precipitation of other diagenetic phases during continued burial (no porosity left to fill). The evidence of halite fully filling in pore space in the past may be seen in Figure 15C and D. However, the Neogene emplacement of hydrocarbons (Jones et al., 2004; Primio and Neumann, 2008) is likely to have dissolved the halite. Wells where no hydrocarbons are found appear to still retain pore-filling halite, but hydrocarbon-bearing sections contain only a small fraction of halite (2%–5%) because of incomplete hydrocarbon placement. Dissolution of halite cements in the channel sands gives rise to megapores (Figure 15C, D) and regenerates porosities of as much as 35%.

Effect of Fluid Overpressure on Porosity Preservation

The effect of pore fluid pressure on porosity preservation has been evaluated in several studies (e.g., Ramm and Bjørlykke, 1994; Gluyas and Cade, 1997; Bloch et al., 2002; Taylor et al., 2010). Fluid overpressures reduce the vertical effective stress, thereby reducing the load borne by the intergranular and cement contacts within buried sands. Three mechanisms have been proposed. First, porosity that would otherwise be lost to compaction is held open by overpressure in a low vertical effective stress regime, resulting in anomalously porous sandstones (Bloch et al., 2002). Second, overpressures have been suggested to limit or prevent significant quartz cementation by inhibiting intergranular pressure solution (e.g., Osborne and Swarbrick, 1999; Swarbrick et al., 2000; Becker et al., 2010). Third, overpressure allows the potential development of secondary porosity or, as in this case here, the recovery of previous porosity that was filled with halite cements.

The early onset of overpressure in the Skagerrak Formation during the Late Triassic was significant in maintaining an early IGV that is higher than would be expected for sandstones at present-day burial depths. We hypothesize that the early fluid overpressures maintained high IGV porosities with increasing burial depth and made a semiclosed, fluid

flow system. Although the amount of overpressure generated in the Late Triassic is small, 2 to 3 MPa (290–435 psi), the magnitude of overpressure at that time, at shallow burial depths, reduced the vertical effective stress by 40% to 60% compared to hydrostatic pore-pressure conditions (Table 3). The early positive effects of fluid overpressure inhibited compaction, maintaining a higher primary porosity. We suggest that early microquartz precipitation stiffened the Skagerrak sands and widespread quartz cementation was further prevented by later chlorite and halite cements. It is widely accepted that halite can deform plastically and dissolve under low differential stress values. (e.g., Davison, 2009; Holt and Powers, 2010; Weisbrod et al., 2012). Where a high IGV porosity, a high pore-fluid pressure, and pore fluids saturated in saline brines exist, halite contributes to the mechanical strength of the Skagerrak sandstones and is not previously recognized in the literature.

The continued ramping up of overpressure since the Late Triassic, with significant increases in the Late Cretaceous, Eocene–Oligocene and from the mid-Pliocene to the present, has resulted in reservoir pore pressures exceeding 60 MPa (8702 psi) and approximately 4500 m (14,764 ft). However, the moderate values of early overpressure at shallow depths were crucial, albeit insufficient on their own, for the maintenance of enhanced porosity with depth. Another necessary factor was the development of robust coatings on detrital grains to preserve intergranular porosity by inhibiting the deposition of pore-filling cements.

CONCLUSIONS

High porosities (as much as 35%) at depths greater than 3200 m (10,499 ft) and temperatures approximately 130°C are found in Triassic Skagerrak fluvial sandstones of the J Block area in the Central Graben. The rate of porosity decline with increasing burial depth has been significantly reduced by a combination of (1) early microquartz cement, (2) Late Triassic fluid overpressure generation, (3) chlorite grain coats and cements, and (4) halite cements.

Early microquartz coatings crystallized from pore waters that were supersaturated with silica contributed significantly to the diagenetic transformation of sand to sandstone during early burial. These coatings stiffened the Skagerrak sands during early burial, enabling them to maintain a high porosity.

Syndepositional evaporites in the mudstone members of the Skagerrak Formation severely reduce permeability to allow fluid overpressure buildup (~5 MPa [725 psi]) where no effective lateral drainage exists.

Authigenic chlorite occurs as grain-coating and pore-filling cements, with all chlorites recognized as magnesium rich. Robust chlorite rims and cements inhibited further quartz cementation on detrital quartz grains. Magnesium rich chlorites were derived as a result of cross-formational flow from the Zechstein sequence and influenced diagenetic reactions from an early stage of burial.

The increasing salinity of pore fluids during burial diagenesis led to pore-filling halite cements in sustained phreatic conditions. The halite pore-filling cements removed most of the remaining porosity and limited precipitation of other diagenetic phases during continued burial (no porosity left to fill). However, the Neogene emplacement of hydrocarbons is likely to have dissolved the halite. Wells where no hydrocarbons are found appear to still contain pore-filling halite, but hydrocarbon-bearing sections contain only a small fraction of halite (2%–5% of pore volume) because of incomplete hydrocarbon placement. Dissolution of halite cements in the channel sands has given rise to megapores and present-day porosities of as much as 35%.

Sandstones that have been subjected to various degrees of diagenesis and vertical effective stress regimes are difficult to interpret, providing a challenge in assessing reservoir quality. However, analysis of the fluvial facies, identification of robust grain coats and halite cements, and modeling overpressure generation in the Skagerrak Formation have enabled us to propose a model that explains the high porosity found in the HPHT reservoirs of the North Sea Central Graben. These results provide a positive step in finding high-porosity facies for deeper targets of approximately 5500 m (18,044 ft) burial depth.

REFERENCES CITED

Aase, N. E., P. A. Bjørkum, and P. H. Nadeau, 1996, The effect of grain-coating microquartz on preservation of reservoir porosity: AAPG Bulletin, v. 80, p. 1654–1673.

Ajdukiewicz, J. M., P. H. Nicholson, and W. L. Esch, 2010, Prediction of deep reservoir quality using early diagenetic process models in the Jurassic Norphlet Formation, Gulf of Mexico: AAPG Bulletin, v. 94, p. 1189–1227, doi:10.1306/04211009152.

Anjos, S. M. C., L. F. De Ros, and C. M. A. Silva, 2003, Chlorite authigenesis and porosity preservation in the Upper Cretaceous marine sandstones of the Santos Basin, offshore eastern Brazil, *in* R. H. Worden and S. Morad, eds., Clay cements in sandstones: Oxford, United Kingdom, Blackwell, p. 291–316.

Archer, S., S. Ward, S. Menad, I. Shahim, N. Grant, H. Sloan, and A. Cole, 2010, The Jasmine discovery, Central North Sea, *in* B. A. Vining and S. C. Pickering, eds., Petroleum geology: From mature basins to new frontiers—Proceedings of the 7th Petroleum Geology Conference: London, United Kingdom, Geological Society, p. 225–243.

Beard, D. C., and P. K. Weyl, 1973, Influence of texture on porosity and permeability of unconsolidated sands: AAPG Bulletin, v. 57, p. 349–369.

Becker, S. P., P. Eichhubl, S. E. Laubach, R. M. Reed, R. H. Lander, and R. J. Bodnar, 2010, A 48 m.y. history of fracture opening, temperature, and fluid pressure: Cretaceous Travis Peak Formation, East Texas Basin: Geological Society of America Bulletin, v. 122, p. 1081–1093, doi:10.1130/B30067.1.

Berger, A., S. Gier, and P. Krois, 2009, Porosity-preserving chlorite cements in shallow-marine volcaniclastic sandstones: Evidence from Cretaceous sandstones of the Sawan gas field, Pakistan: AAPG Bulletin, v. 95, p. 595–615, doi:10.1306/01300908096.

Bishop, D., 1996, Regional distribution and geometry of salt diapirs and supra-Zechstein group faults in the western and central North Sea: Marine and Petroleum Geology, v. 14, p. 355–364, doi:10.1016/0264-8172(95)00081-X.

Bjørlykke, K., and P. Aagaard, 1992, Clay minerals in North Sea sandstones, *in* D. W. Houseknecht and E. D. Pittman, eds., Origin, diagenesis, and petrophysics of clay minerals in sandstones: Tulsa, Oklahoma, SEPM, p. 65–80.

Bjørlykke, K., and K. Gran, 1994, Salinity variations in North Sea formation waters: Implications for large-scale fluid movements: Marine and Petroleum Geology, v. 11, p. 5–9, doi:10.1016/0264-8172(94)90003-5.

Bloch, S., R. H. Lander, and L. M. Bonnell, 2002, Anomalously high porosity and permeability in deeply buried sandstone reservoirs: Origin and predictability: AAPG Bulletin, v. 86, p. 301–328.

Burley, S. D., J. Mullis, and A. Matter, 1989, Timing diagenesis in the Tartan reservoir (JK North Sea): Constraints from combined cathodoluminescence microscopy and fluid inclusion studies: Marine and Petroleum Geology, v. 6, p. 98–120, doi:10.1016/0264-8172(89)90014-7.

Cardell, C., A. Yebra, and R. E. Van Grieken, 2002, Applying digital image processing to SEM-EDX and BSE images to determine and quantify porosity and salts with depth in porous media: Microchimica Acta, v. 140, p. 9–14.

Carr, A. D., 2003, Thermal history model for the south Central Graben, North Sea, derived using both tectonics and maturation: International Journal of Coal Geology, v. 54, p. 3–19.

Cartwright, J. A., S. A. Stewart, and J. Clark, 2001, Salt dissolution and salt-related deformation of the Forth Approaches Basin, UK North Sea: Marine and Petroleum Geology, v. 18, p. 757–778, doi:10.1016/S0264-8172(01)00019-8.

Clark, J. A., J. A. Cartwright, and S. A. Stewart, 1999, Mesozoic dissolution tectonics on the West Central Shelf, UK Central North Sea: Marine and Petroleum Geology, v. 16, p. 283–300, doi:10.1016/S0264-8172(98)00040-3.

Darby, D., R. S. Haszeldene, and G. Couples, 1996, Pressure cells and pressure seals in the central North Sea: Marine and Petroleum Geology, v. 13, p. 865–878, doi:10.1016/S0264-8172(96)00023-2.

Davison, I., 2009, Faulting and fluid flow through salt: Journal of the Geological Society, v. 166, p. 205–216, doi:10.1144/0016-76492008-064.

Davison, I., I. Alsop, P. Birch, C. Elders, N. Evans, H. Nicholson, P. Rorison, D. Wade, J. Woodward, and M. Young, 2000, Geometry and late-stage structural evolution of Central Graben salt diapirs, North Sea: Marine and Petroleum Geology, v. 17, p. 499–522, doi:10.1016/S0264-8172(99)00068-9.

de Jong, M., D. Smith, S. D. Nio, and N. Hardy, 2006, Subsurface correlation of the Triassic of the UK southern Central Graben: New look at an old problem: First Break, v. 24, no. 6, p. 103–109.

Dixon, S. A., D. M. Summers, and R. C. Surdam, 1989, Diagenesis and preservation of porosity in Norphlet Formation (Upper Jurassic), southern Alabama: AAPG Bulletin, v. 73, p. 707–728.

Dowey, P. J., D. M. Hodgson, and R. H. Worden, 2012, Prerequisites, processes, and prediction of chlorite grain coatings in petroleum reservoirs: A review of subsurface examples: Marine and Petroleum Geology, v. 32, p. 63–75, doi:10.1016/j.marpetgeo.2011.11.007.

Ehrenberg, S. N., 1989, Assessing the relative importance of compaction processes and cementation to reduction of porosity in sandstones: Discussion: AAPG Bulletin, v. 73, p. 1274–1276.

Fisher, M. J., and D. C. Mudge, 1998, Triassic, *in* K. W. Glennie, ed., Petroleum geology of the North Sea: Basic concepts and recent advances: Oxford, United Kingdom, Blackwell, p. 212–244.

Gaarenstroom, L., R. A. J. Tromp, M. C. de Jong, and A. M. Brandenburg, 1993, Overpressure in the central North Sea: Implications for trap integrity and drilling safety, *in* J. R. Parker, ed., Petroleum geology of northwest Europe: Proceedings of the 4th Conference: London, United Kingdom, Geological Society, v. 2, p. 1305–1313.

Gaupp R., A. Matter, J. Platt, K. Ramseyer, and J. Walzebuck, 1993, Diagenesis and fluid evolution of deeply buried Permian (Rotliegende) gas reservoirs, Northwest Germany: AAPG Bulletin, v. 77, p. 1111–1128.

Glennie, K. W., ed., 1998, Petroleum geology of the North Sea: Basic concepts and recent advances, 4th ed., Oxford, United Kingdom, Blackwell, 636 p.

Gluyas, J. G., and C. A. Cade, 1997, Prediction of porosity in compacted sands, *in* J. A. Kupecz, J. G. Gluyas, and C. A. Cade, eds., Reservoir quality prediction in sandstones and carbonates: AAPG Memoir 69, p. 19–28.

Goldsmith, P. J., B. Rich, and J. Standring, 1995, Triassic correlation and stratigraphy in the south Central Graben, UK North Sea, *in* S. Boldy, ed., Permian and Triassic rifting in northwest Europe: Geological Society (London) Special Publication 91, p. 123–143.

Goldsmith, P. J., G. Hudson, and P. van Veen, 2003, Triassic, *in* D. Evans, C. Graham, A. Armour, and P. Bathurst, eds., The millennium atlas: Petroleum geology of the central and northern North Sea: London, United Kingdom, Geological Society, p. 105–127.

Gowers, M. B., and A. Sæbøe, 1985, On the structural evolution of the Central Trough in the Norwegian and Danish sectors of the North Sea: Marine and Petroleum Geology, v. 2, p. 298–318, doi:10.1016/0264-8172(85)90026-1.

Grove, C., and D. A. Jerram, 2011, jPOR: An ImageJ macro to quantify total optical porosity from blue-stained thin sections: Computers and Geosciences, v. 37, p. 1850–1859, doi:10.1016/j.cageo.2011.03.002.

Haddad, S. C., R. H. Worden, D. J. Prior, and P. C. Smalley, 2006, Quartz cement in the Fontainebleau Sandstone, Paris Basin, France: Crystallography and implication for mechanisms of cement growth: Journal of Sedimentary Research, v. 76, p. 244–256, doi:10.2110/jsr.2006.024.

Hammer, E., M. B. E. Mork, and A. Naess, 2010, Facies controls on the distribution of diagenesis and compaction in fluvial-deltaic deposits: Marine and Petroleum Geology, v. 27, p. 1737–1751, doi:10.1016/j.marpetgeo.2009.11.002.

Haszeldene, R. S., M. Wilkinson, D. Darby, C. I. Macaulay, G. D. Couples, A. E. Fallick, C. G. Fleming, R. N. T. Stewart, and G. McAulay, 1999, Diagenetic porosity creation in an overpressured graben, *in* A. J. Fleet and S. A. Boldy, eds., Petroleum geology of northwest Europe: Proceedings of the 5th Conference: London, United Kingdom, Geological Society, p. 1339–1350.

Hendry, J. P., M. Wilkinson, A. E. Fallick, and R. S. Haszeldene, 2000, Ankerite cementation in deeply buried Jurassic sandstone reservoirs of the central North Sea: Journal of Sedimentary Research, v. 70, p. 227–239, doi:10.1306/2DC4090D-0E47-11D7-8643000102C1865D.

Hodgson, N. A., J. Farnsworth, and S. J. Fraser, 1992, Salt related tectonics, sedimentation and hydrocarbon plays in the Central Graben, North Sea, UKCS, *in* R. F. P. Hardman, ed., Exploration Britain: Geological Society (London) Special Publication 67, p. 31–63.

Hoiland, O., J. Kristensen, and T. Monsen, 1993, Mezozoic evolution of the Jaeren High area, Norwegian central North Sea, *in* J. R. Parker, ed., Petroleum geology of Northwest Europe: Proceedings of the 4th Conference: London, United Kingdom, Geological Society, v. 2, p. 1189–1195.

Holm, G. M., 1998, Distribution and origin of overpressure in the Central Graben of the North Sea, *in* B. E. Law, G. F. Ulmishek, and V. I. Slavin, eds., Abnormal pressures in hydrocarbon environments: AAPG Memoir 70, p. 123–144.

Holt, R. M., and D. W. Powers, 2010, Evaluation of halite dissolution at a radioactive waste disposal site, Andrews County, Texas: Geological Society of America Bulletin, v. 122, p. 1989–2004.

Isaksen, G. H., 2004, Central North Sea hydrocarbon systems: Generation, migration, entrapment, and thermal degradation of oil and gas: AAPG Bulletin, v. 88, p. 1545–1572, doi:10.1306/06300403048.

Jackson, C. A. L, K. E. Kane, and E. Larsen, 2010, Structural evolution of minibasins on the Utsira High, northern North Sea; Implications for Jurassic sediment dispersal and reservoir distribution: Petroleum Geoscience, v. 16, p. 105–120, doi:10.1144/1354-079309-011.

Jones, A. D., H. A. Auld, T. J. Carpenter, E. Fetkovich, I. A. Palmer, E. N. Rigatos, and M. W. Thompson, 2004, Jade field: An innovative approach to high-pressure/high-temperature field development, *in* A. G. Doré and B. A. Vining, eds., Petroleum geology: North-west Europe and global perspectives: Proceedings of the 6th Petroleum Geology Conference: London, United Kingdom, Geological Society, p. 1–16.

Kape, S., O. Diaz De Souza, I. Bushnaq, M. Hayes, and I. Turner, 2010, Predicting production behaviour from deep HPHT Triassic reservoirs and the impact of sedimentary architecture on recovery, *in* B. A. Vining and S. C. Pickering, eds., Petroleum geology: From mature basins to new frontiers—Proceedings of the 7th Petroleum Geology Conference: London, United Kingdom, Geological Society, p. 405–417.

Katsube, T. J., J. Bloch, and W. C. Cox, 1999a, The effect of diagenetic alteration on shale pore-structure and its implications for abnormal pressures and geophysical signatures, *in* A. Mitchell and D. Grauls, eds., Overpressure in petroleum exploration: Proceedings of the workshop: Bulletin Centre Recherche Elf Exploration and Production Memoir 22, p. 49–54.

Katsube, T. J., S. R. Dallimore, T. Uchida, K. A. Jenner, T. S. Collett, and S. Connell, 1999b, Petrophysical environment of sediments hosting gas-hydrate, JAPEX/JNOC/GSC Mallik 2L-38 gas hydrate research well, *in* S. R. Dallimore, T. Uchida, and T. S. Collett, eds., Scientific results from JAPEX/JNOC/GSC Mallik 2L-38 gas hydrate research well, Mackenzie delta, North West Territories, Canada: Geological Survey of Canada Bulletin 544, p. 109–124.

Keller, T., R. Bayes, H. Auld, and M. Lines, 2005, Judy field: Rejuvenation through a second phase of drilling, Geological Society (London) Petroleum Geology Conference Series 6, p. 651–661, doi:10.1144/0060651.

Kugler, R. L., and A. McHugh, 1990, Regional diagenetic variation in Norphlet Sandstone: Implications for reservoir quality and the origin of porosity: Gulf Coast Association of Geological Societies Transactions, v. 40, p. 411–423.

Laier, T., and L. B. Nielsen, 1989, Cementing halite in Triassic Bunter Sandstone (Tønder, southwest Denmark) as a result of hyperfiltration of brines: Chemical Geology, p. 353–363, doi:10.1016/0009-2541(89)90103-4.

Lander, R. H., R. E. Larese, and L. M. Bonnell, 2008, Towards more accurate quartz cement models: The importance of euhedral versus noneuhedral growth rates: AAPG Bulletin, v. 92, p. 1537–1563, doi:10.1306/07160808037.

Lervik, K. S., 2006, Triassic lithostratigraphy of the northern North Sea Basin: Norwegian Journal of Geology, v. 86, p. 93–116.

Lines, D. M., and H. A. Auld, 2004, A petroleum charge model for the Judy and Joanne fields, central North Sea: Application to exploration and field development, *in* J. M. Cubitt, W. A. England, and S. Larter, eds., Understanding petroleum reservoirs: Towards an integrated reservoir engineering and geochemical approach: Geological Society (London) Special Publication 237, p. 175–206.

Lubanzadio, M., N. R. Goulty, and R. E. Swarbrick, 2002, Variation of velocity with effective stress in chalk: Null result from North Sea well data: Marine and Petroleum Geology, v. 19, p. 921–927.

Maast, T. E., J. Jahren, and K. Bjørlykke, 2011, Diagenetic controls on reservoir quality in Middle to Upper Jurassic sandstones in the South Viking Graben, North Sea: AAPG Bulletin, v. 95, p. 1937–1958, doi:10.1306/03071110122.

Mallon, A. J, and R. E. Swarbrick, 2008, Diagenetic characteristics of low-permeability, nonreservoir chalks from the central North Sea: Marine and Petroleum Geology, v. 25, p. 35–45.

Matthews, W. J., G. J. Hampson, B. D. Trudgill, and J. R. Underhill, 2007, Controls on fluvio-lacustrine reservoir distribution and architecture in passive salt diapir provinces: Insights from outcrop analogs: AAPG Bulletin, v. 91, p. 1367–1403, doi:10.1306/05310706123.

McCartney, R. A., P. Winefield, P. Webb, and O. Kuhn, 2004, Spatial variations in the composition of formation waters from the central North Sea: Implications for fluid flow in the deep high-pressure high-temperature hydrocarbon play, *in* J. M. Cubitt, W. A. England, and S. R. Larter, eds., Understanding petroleum reservoirs: Towards an integrated reservoir engineering and geochemical approach: Geological Society (London) Special Publication 237, p. 283–303.

McKie, T., and P. Audretsch, 2005, Depositional and structural controls on Triassic reservoir performance in the Heron Cluster, ETAP, central North Sea, *in* A. G. Doré and B. A. Vining, eds., Petroleum geology: North-west Europe and global perspectives: Proceedings of the 6th Petroleum Geology Conference: London, United Kingdom, Geological Society, p. 285–297.

McKie, T., and B. Williams, 2009, Triassic palaeogeography and fluvial dispersal across the northwest European basins: Geological Journal, v. 44, p. 711–741, doi:10.1002/gj.1201.

McKie, T., S. J. Jolley, and M. B. Kristensen, 2010, Stratigraphic and structural compartmentalization of dryland fluvial reservoirs: Triassic Heron Cluster, central North Sea, *in* S. J. Jolley, Q. J. Fisher, R. B. Ainsworth, P. J. Vrolijk, and S. Delisle, eds., Reservoir compartmentalization: Geological Society (London) Special Publication 347, p. 165–198.

Megson, J., and R. Hardman, 2001, Exploration for and development of hydrocarbons in the chalk of the North Sea: A low-permeability system: Petroleum Geoscience, v. 7, p. 3–12.

Midttømme, K., E. Roaldset, and P. Aagaard, 1998, Thermal conductivity of selected claystones and mudstones from England: Clay Minerals, v. 33, p. 131–145.

Morad, S., K. Al-Ramadan, J. M. Ketzer, and L. F. De Ros, 2010, The impact of diagenesis on the heterogeneity of sandstone reservoirs: A review of the role of depositional facies and sequence stratigraphy: AAPG Bulletin, v. 94, p. 1267–1309, doi:10.1306/04211009178.

Osborne, M. J., and R. E. Swarbrick, 1999, Diagenesis in North Sea HPHT clastic reservoirs: Consequences for porosity and overpressure prediction: Marine and Petroleum Geology, v. 16, p. 337–353, doi:10.1016/S0264-8172(98)00043-9.

Peltonen, C., Ø. Marcussen, K. Bjørlykke, and J. Jahren, 2009, Clay mineral diagenesis and quartz cementation in mudstones: The effects of smectite to illite reaction on rock properties: Marine and Petroleum Geology, v. 26, p. 887–898, doi:10.1016/j.marpetgeo.2008.01.021.

Penge, J., J. W. Munns, B. Taylor and T. M. F. Windle, 1999, Rift-raft tectonics: Examples of gravitational tectonics from the Zechstein basins of northwest Europe, *in* A. J. Fleet and S. A. Boldy, eds., Petroleum geology of northwest Europe: Proceedings of the 5th Conference: London, United Kingdom, Geological Society, p. 201–213.

Pittman, E. D., R. E. Larese, and M. T. Heald, 1992, Clay coats: Occurrence and relevance to preservation of porosity in sandstones: SEPM Special Publication 47, p. 241–255.

Primio, D. R., and V. Neumann, 2008, HPHT reservoir evolution: A case study from Jade and Judy fields, Central Graben, UK North Sea: International Journal of Earth Sciences, v. 97, p. 1101–1114, doi:10.1007/s00531-007-0206-y.

Purvis, K., 1992, Lower Permian Rotliegend sandstones, southern North Sea: A case study of sandstone diagenesis in evaporite-associated sequences: Sedimentary Geology, v. 77, p. 155–171, doi:10.1016/0037-0738(92)90123-9.

Ramm, M., and K. Bjørlykke, 1994, Porosity/depth trends in reservoir sandstones: Assessing the quantitative effects of varying pore-pressure, temperature history and mineralogy, Norwegian Shelf data: Clay Minerals, v. 29, p. 475–490, doi:10.1180/claymin.1994.029.4.07.

Smith, R. I., N. Hodgson, and M. Fulton, 1993, Salt control on Triassic reservoir distribution, UKCS central North Sea, *in* J. R. Parker, ed., Petroleum geology of northwest Europe: Proceedings of the 4th Conference: London, United Kingdom, Geological Society, v. 1, p. 547–557.

Swarbrick, R. E., M. J. Osborne, D. Grunberger, G. S. Yardley, G. Macleod, A. C. Aplin, S. R. Larter, I. Knight, and H. A. Auld, 2000, Integrated study of the Judy field (Block 30/7a): An overpressured central North Sea oil/gas field: Marine and Petroleum Geology, v. 17, p. 993–1010, doi:10.1016/S0264-8172(00)00050-7.

Taylor, T. R., M. R. Giles, L. A. Hathon, T. N. Diggs, N. R. Braunsdorf, G. V. Birbiglia, M. G. Kittridge, C. I. Macaulay, and I. S. Espejo, 2010, Sandstone diagenesis and reservoir quality prediction: Models, myths, and reality: AAPG Bulletin, v. 94, p. 1093–1132, doi:10.1306/04211009123.

Thyne, G., B. P. Boudreau, M. Ramm, and R. E. Midtbo,

2001, Simulation of potassium feldspar dissolution and illitization in the Statfjord Formation, North Sea: AAPG Bulletin, v. 85, p. 621–635.

Warren, E. A., P. C. Smalley, and R. J. Howarth, 1994, Compositional variation of North Sea formation water, *in* E. A. Warren and P. C. Smalley, eds., North Sea Formation Waters Atlas: Geological Society (London) Memoir 15, p. 119–208.

Weibel, R., 1998, Diagenesis in oxidising and locally reducing conditions: An example from the Triassic Skagerrak Formation, Denmark: Sedimentary Geology, v. 121, p. 259–276, doi:10.1016/S0037-0738(98)00085-2.

Weibel, R., 1999, Effects of burial on the clay assemblages in the Triassic Skagerrak Formation, Denmark: Clay Minerals, v. 34, p. 619–635, doi:10.1180/000985599546488.

Weibel, R., and H. Friis, 2004, Opaque minerals as keys for distinguishing oxidising and reducing diagenetic conditions in the Lower Triassic Bunter Sandstone, North German Basin: Sedimentary Geology, v. 169, p. 129–149, doi:10.1016/j.sedgeo.2004.05.004.

Weisbrod, N., C. Alon-Mordish, E. Konen, and Y. Yechieli 2012, Dynamic dissolution of halite rock during flow of diluted saline solutions: Geophysical Research Letters 39, L09404, 7 p., doi:10.1029/2012GL051306.

Wilkinson, M., R. S. Haszeldene, and A. E. Fallick, 2006, Hydrocarbon filling and leakage history of a deep geopressured sandstone, Fulmar Formation, United Kingdom North Sea: AAPG Bulletin, v. 90, p. 1945–1961, doi:10.1306/06270605178.

Willis, B. J., and H. Tang, 2010, Three-dimensional connectivity of point-bar deposits: Journal of Sedimentary Research, v. 80, p. 440–454, doi:10.2110/jsr.2010.046.

Yardley, G. S., and R. E. Swarbrick, 2000, Lateral transfer: A source of additional overpressure: Marine and Petroleum Geology, v. 17, p. 523–538, doi:10.1016/S0264-8172(00)00007-6.